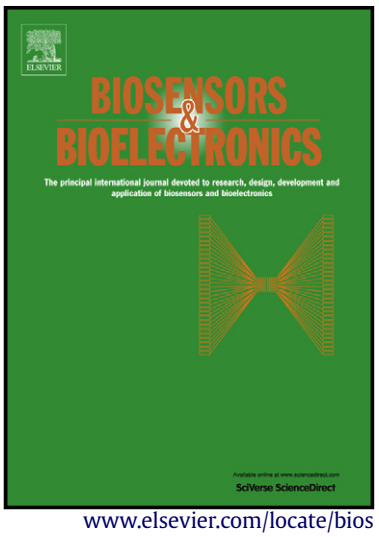

www.elsevier.com/locate/bios

Integrated planar optical waveguide interferometer biosensors: a comparative review

Peter Kozma, Florian Kehl, Eva Ehrentreich-Förster, Christoph Stamm, Frank F. Bier

PII: S0956-5663(14)00137-7
DOI: http://dx.doi.org/10.1016/j.bios.2014.02.049
Reference: BIOS6594

To appear in: *Biosensors and Bioelectronics*

Received date: 26 November 2013
Revised date: 10 February 2014
Accepted date: 11 February 2014

Cite this article as: Peter Kozma, Florian Kehl, Eva Ehrentreich-Förster, Christoph Stamm, Frank F. Bier, Integrated planar optical waveguide interferometer biosensors: a comparative review, *Biosensors and Bioelectronics,* http://dx.doi.org/10.1016/j.bios.2014.02.049

Integrated planar optical waveguide interferometer biosensors: a comparative review

Peter Kozma,[1,*] Florian Kehl,[2] Eva Ehrentreich-Förster,[1] Christoph Stamm,[3] Frank F. Bier[1]

1) Fraunhofer Institute for Biomedical Engineering (IBMT), Am Mühlenberg 13, 14476 Potsdam-Golm, Germany
2) Laboratory of Biosensors and Bioelectronics (LBB), Swiss Federal Institute of Technology (ETH), Gloriastrasse 35, 8092 Zürich, Switzerland
3) Zurich University of Applied Sciences (ZHAW), School of Engineering, Institute of Applied Mathematics and Physics (IAMP), Technikumstrasse 9, 8400 Winterthur, Switzerland

* Corresponding author: Peter Kozma (peter.kozma@ibmt.fraunhofer.de)

Peter Kozma is on leave from the Institute of Technical Physics and Materials Science (MFA) of the Hungarian Academy of Sciences (HAS).

Abstract

Integrated planar optical waveguide interferometer biosensors are advantageous combinations of evanescent field sensing and optical phase difference measurement methods. By probing the near surface region of a sensor area with the evanescent field of a guided mode, any change of the refractive index of the probed volume induces a phase shift of the mode compared to a reference field typically of a mode propagating through the reference arm of the same waveguide structure. The interfering fields of these modes produce an interference signal detected at the sensor's output, whose alteration is proportional to the refractive index change. This signal can be recorded, processed and related to e.g. the concentration of an analyte in the solution of interest. Although this sensing principle is relatively simple, studies about integrated planar optical waveguide interferometer biosensors can mostly be found in the literature covering the past twenty years. During these two decades, several members of this sensor family have been introduced, which have remarkably advantageous properties. These entail label-free and non-destructive detection, outstandingly good sensitivity and

detection limit, cost-effective and simple production, ability of multiplexing and miniaturization. Furthermore, these properties lead to low reagent consumption, short analysis time and open prospects for point-of-care applications. The present review collects the most relevant developments of the past twenty years categorizing them into two main groups, such as common- and double path waveguide interferometers. In addition, it tries to maintain the historical order as it is possible and it compares the diverse sensor designs in order to reveal not only the development of this field in time, but to contrast the advantages and disadvantages of the different approaches and sensor families, as well.

Keywords: waveguide, common- and double path interferometer, biosensor, evanescent field, label-free detection

1. Introduction

With the development of the enzyme electrode in 1967, Updike and Hicks presented the first biosensor and hereby demonstrated its huge prospects in medicine and biotechnology (Updike and Hicks, 1967). With this achievement, they started a continuous and ongoing development process within the field of biosensing (Chambers et al., 2008). Although, during these almost 50 years, numerous new sensor designs with better and better properties have been published and commercialized, the need for decreasing size and cost, but improving sensitivity, detection limit, specificity and stability still challenges today's scientists and engineers. Miniaturized, fast, cheap, easy-to-use and reliable glucose biosensors already make the life more comfortable and safe for those, who are suffering from diabetes (Oliver et al., 2009). Beyond the biomedical applications of e.g. pregnancy, bacterial infection, cholesterol and troponin T quick tests (Holford et al., 2012; Justino et al., 2010), the new approaches of biosensorics open up new opportunities; they are e.g. widely used in forensic medicine (alcohol, drug, doping tests, etc.) and industry (pharmaceuticals, water-, food quality, etc.), as well (Alocilja and Radke, 2003; Fan et al., 2008; Klenkar and Liedberg, 2008; Lazcka et al., 2007).

The sensitive and specific detection of biological substances of molecular weights even less than 500 Da at a concentration of typically less than a few pg/ml, is still not trivial today in a sample, where numerous other molecules may also be present dissolved in a significantly larger quantity (Cunningham, 2009). The interest in reliable and cost-effective transducers,

namely biosensors, which are able to convert the recognition of these tiny biological entities, i.e., targets to an amplified signal, still remains (Kozma et al., 2013).

Today, the most sensitive biosensors are based on fluorescent, radioactive or magnetic labeling, since following the signal produced by the label, the binding or the presence of even an individual molecule can be detected in the observed volume or on the studied surface (Alivisatos, 2001; Jain, 2005). Beyond this indubitable advantage, unfortunately they are suffering from numerous drawbacks compared to label-free techniques. For instance, the chemical procedure of labeling is rather expensive, time and labor intensive. The number of fluorophores on the molecules cannot be controlled precisely, which leads to a fluorescence signal bias. Furthermore, the presence of these anchored tags could have a not-negligible effect on the molecules, thus on the experimental results, as well (Cooper, 2002; Fan et al., 2008). As a consequence, the label-free techniques are very important mates of labeling ones. Moreover, they have better future perspectives, since they offer sensitive, specific and fast measurements without the abovementioned drawbacks. By immobilizing recognition elements and by mounting a flow-cell onto a label-free sensor chip, quantitative, in situ and real time detection of the target molecules or kinetic measurements of molecular interactions is possible.

Regarding the competition of label-free signal transducers such as mass-sensitive, temperature-sensitive, electrochemical and optical biosensors, the optical methods are dominating both the research literature and the market (Lazcka et al., 2007; O'Malley, 2008). The reason is mainly that optical methods are merging the advantages of other label-free techniques into a cost-effective way. The binding of the target analytes is detected in their natural form using low-power electric field in or close to the visible range with neither destructive nor considerable manipulative effect on the experiment. The sampling rate and the detection limit of surface mass density changes are outstandingly good, which allows a very efficient real-time monitoring. In most cases, performing parallel measurements is straightforward due to their ability of multiplexing for multi-parameter analysis (Cunningham, 2009). The technological demands for the fabrication of these transducers are relatively low and by batch manufacturing the optical elements in a more cost-effective and more compact way, their ongoing miniaturization leads to novel possibilities, towards even lower reagent consumption, shorter analysis time and consequently towards point-of-care applications.

The working principle of these devices is depicted in Figure 1 and can briefly be summarized as follows: binding target molecules with higher refractive index are displacing the lower

refractive index ambient (e.g. water or buffer) of the biological or biologically derived recognition elements, such as e.g. receptors, antibodies, aptamers, nucleic acids, enzymes or molecular imprints (Chambers et al., 2008), which are integrated or associated with an optical signal transducer (see the following chapters) (Turner, 2000). As a consequence, the value of this physical parameter is changing locally, which has an effect on the related optical quantities, such as e.g. phase velocity of the propagating electromagnetic wave, polarization state, light intensity and wavelength (Cunningham, 2009; Fan et al., 2008). The optical signal transducer amplifies this variation to a measurable, typically electric signal. All sensor configurations presented in this review are utilizing this relatively simple, but very sensitive principle.

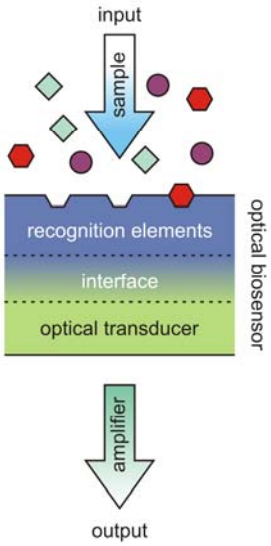

Figure 1: *Schematic working principle of label-free optical biosensors.* Surface immobilized recognition elements specifically bind the sample of interest, commonly one or several target molecules within a complex sample. The resulting mass adsorption and displacement of the surrounding medium results in a change of the local refractive index at the sensor surface. This variation has a direct effect on the physical properties of the interrogating electromagnetic wave, which can be amplified by the optical transducer.

2. The scope of this review

The aim of this review is not to summarize the recent developments in the whole field of label-free optical methods. It tries to keep the focus only on a sub-group of optical waveguide based techniques; the integrated planar optical waveguide interferometer biosensors. With special emphasis on their transduction mechanism, namely on optical structures and their interaction with the analyte, the review presents the most important development directions and achievements of the last twenty years towards the modern point-of-care waveguide interferometer applications. Detailed reviews of chemical modification and bioconjugation of sensor surfaces can be found in Refs. (Bañuls et al., 2013; Hunt and Armani, 2014).

Waveguide interferometers have particular importance, since the smart combination of two very sensitive methods, the waveguiding and the interferometry techniques, resulted in a next generation of biosensors. By utilizing the advantages of these two approaches, they do not lose on mechanical stability, reliability, ability in mass production and miniaturization. Consequently, they are well-suited for point-of-care applications (Duval et al., 2012a). Without the need of directed transport of biomolecules onto individual nanoscale sensor structures, waveguide interferometers in practice typically have one or even two orders of magnitude better detection limit for surface mass density and refractive index changes calculated for a macroscopic sensor area than e.g., microring resonators, silicon wires, slot-waveguides or photonic crystals and grating coupler sensors, furthermore, they can be characterized theoretically as well as practically with higher sensitivity potential even in comparison with surface plasmon resonance spectroscopy (Brandenburg, 1996; Ciminelli et al., 2013; Estevez et al., 2012; Lukosz, 1991; Sheehan and Whitman, 2005; Squires et al., 2008; Zinoviev et al., 2008). Moreover, other significant advantages of these techniques are their broad dynamic range and long interaction length. For instance, surface plasmon resonance spectroscopes and output grating coupler sensors have a trade-off between the dynamic range and resolution (Cottier, 2004; Homola et al., 1999). The dynamic range of input grating coupler sensors can be limited by e.g. mechanical or optical constrains, such as the range of e.g. angle of incidence or wavelength tuning (Cottier et al., 2003). In contrast, a waveguide interferometer based refractometry measurement can be typically performed continuously even in the range of the refractive index of vacuum and that of the waveguide film. On the macroscopic sensor surfaces of waveguide interferometers, the measuring light can interact with the sample over a typical length of several millimeters up to a few

centimeters, which outperforms in this way e.g. the microring resonators and silicon wires (Estevez et al., 2012).

Of course, the waveguide interferometers also lack specific features compared to the other sensors, they also have important drawbacks originated from their working principle. One of them is that only relative parameter values (related to a reference) can be gained from a waveguide interferometer-based measurement. To reveal absolute parameter values is not straightforward today. Additionally, they are highly sensitive for wavelength instabilities, consequently, cost-intensive temperature-stabilized coherent light sources have to be applied to avoid wrong interpretation of the measurement. Furthermore, in order to suppress the non-negligible effects of mechanical vibrations and temperature changes, the sensor unit has to be stabilized and properly isolated from the environment, which is typically a bar to device miniaturization. As it will be seen later on by the introduction of individual sensor configurations, a further imperfectness of the "state of the art" is that simultaneous spectroscopic, multimode and/or multi-polarization measurements are typically not straightforward today. The future challenge is to design waveguide interferometer sensor systems, which are capable of detecting and investigating bio-chemical reactions with improved sensitivity and detection limit, without the aforementioned disadvantages and in a way suitable for point-of-care applications.

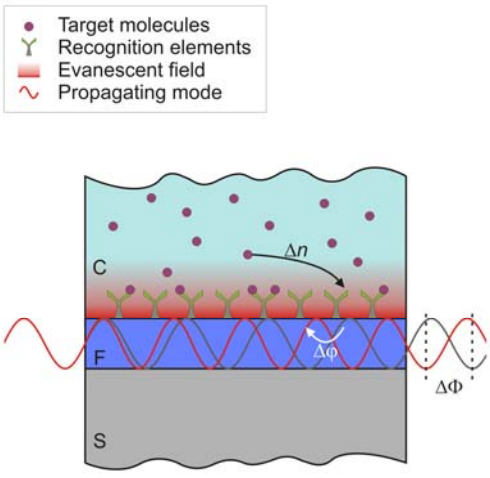

Figure 2: *Schematic working principle of label-free planar optical waveguide interferometer biosensors.* The binding of target molecules to recognition elements causes a local refractive index change, Δn, of the cover, C, in immediate proximity of the waveguide film, F. This change induces a phase shift, $\Delta\varphi$, of the guided mode (red wave) propagating underneath, since this region is probed with evanescent field. The resulting phase difference, $\Delta\Phi$, between this mode and a reference one (gray wave) is detected based on their interference.

Despite the significant differences in their realization (see later in the following chapters), waveguide interferometers follow a common basic working principle: One or several modes are propagating in a waveguide, while their evanescent field is probing the near surface region, where any change of the refractive index induces phase shifts of the modes. Combining the phase shifted modes with each other or combining a phase shifted mode with a reference one, an intensity variation, namely, an interference signal can be measured at the sensor's output (Figure 2). This signal can be further processed and related to the quantity of the analyte adsorbed or the change of the cover refractive index, respectively.

3. Theoretical Approach of Planar Optical Waveguide Interferometers

3.1. Young and Mach-Zehnder Interferometry

The famous double-slit experiment of T. Young published in 1804 in Ref. (Young, 1804) played a crucial role in the general acceptance of the wave theory of light. Moreover, it later inspired numerous fields of physics from classical optics to modern quantum physics and helped us to understand our world more profoundly. The experiment, which has demonstrated that the light of a point source passing through two thin and closely spaced slits produces an interference pattern in the far-field, has effectively been exploited in biosensorics as Young interferometers. An early application of the interference has also had an enormous impact on this field of sciences. About 90 years later, L.Z. Mach and L.Z. Zehnder independently published that collimated beams of a light source can be applied for measuring refractive index changes (Mach, 1892; Zehnder, 1891). Both Mach-Zehnder and Young interferometers utilize the wave nature of light for detecting the changes of the optical properties of a sample and are consequently similar regarding their working principle. In a modern interferometer, the polarized light of a coherent and monochromatic source is split into two beams to propagate independently in the two interferometer arms. One of the arms, the so-called sample or sensor arm, interacts with the sample of interest. Any change of the sample shifts the phase of this beam compared to the one of the reference arm, which is either insulated from the environment or interacts with a reference sample. The difference between the two interferometers is basically the way how the interference of the two beams is produced. In a Mach-Zehnder interferometer, the beams are recombined by directing them again onto the same root towards a photodetector (Figure 3a). Due to the wave nature of light, the measured

intensity, I, is a periodic function of the phase shift difference, $\Delta\Phi$, of the beams passed through the two different paths (beam No. 1 and 2) (Jenkins and White, 1957a):

$$I = I_1 + I_2 + 2\sqrt{I_1 I_2}\cos(\Delta\Phi). \tag{3.1}$$

Equation 3.1 is based on the fact that the intensity is proportional to the square of the resulting amplitude of two interfering waves. The phase shift difference of the beams of the two different paths, L_1 and L_2, can be calculated as:

$$\Delta\Phi = k_0\left(\int_{L_1} n(\underline{r})d\underline{r} - \int_{L_2} n(\underline{r})d\underline{r}\right), \tag{3.2}$$

where $k_0 = 2\pi/\lambda_0$ is the wave number and λ_0 is wavelength measured both in vacuum and $n(\underline{r})$ is the refractive index of the medium at point $\underline{r}$.

The beams of a Young interferometer are projected from two closely spaced secondary sources (representing the two slits of Young's experiment) onto a detector array, where not a single intensity, but an interference pattern, a so-called interferogram is detected (Figure 3b). The optical path length difference of the rays originating from the two sources is varying along the y axis of the detector, which is chosen to be parallel to the axis defined by the two secondary sources. For this case, equation 3.1 can be rewritten as (Jenkins and White, 1957b):

$$I(y) = \gamma(y)\left[I_1 + I_2 + 2\sqrt{I_1 I_2}\cos(\Lambda y + \Delta\Phi)\right], \tag{3.3}$$

where $\Lambda = l/kd$ is the spatial period of the fringes, $k = k_0 n = 2\pi/\lambda$ is the wave number in medium, d and l are denoting the spacing of the two sources and the distance of the plane of the sources and the detector surface, respectively, and λ is the wavelength in medium. Furthermore, a form factor $\gamma(y) = \sin^2(\chi)/\chi^2$ representing the diffraction on a single slit of width b modulates the intensities of the interference fringes, where $\chi = kby/2l$.

In case of integrated Mach-Zehnder as well as Young interferometers, at least the sensor arm (or at least its sensing region) is realized in an integrated optical waveguide structure. In this manner, one can further differentiate between fully integrated and hybrid (partially integrated) interferometers (see examples in the following chapters). This kind of integration has the advantage that a well-defined sensor surface can be created at a particular region of the waveguide, where sensing with evanescent field, i.e., sensitive near-surface (bio)detection can be performed. In contrast to integrated Mach-Zehnder interferometry, where the actual intensity is related to the phase difference of the two beams, the position of the interference fringes is proportional to the phase difference in case of integrated Young interferometry. This methodical difference allows a clear distinction between the two approaches.

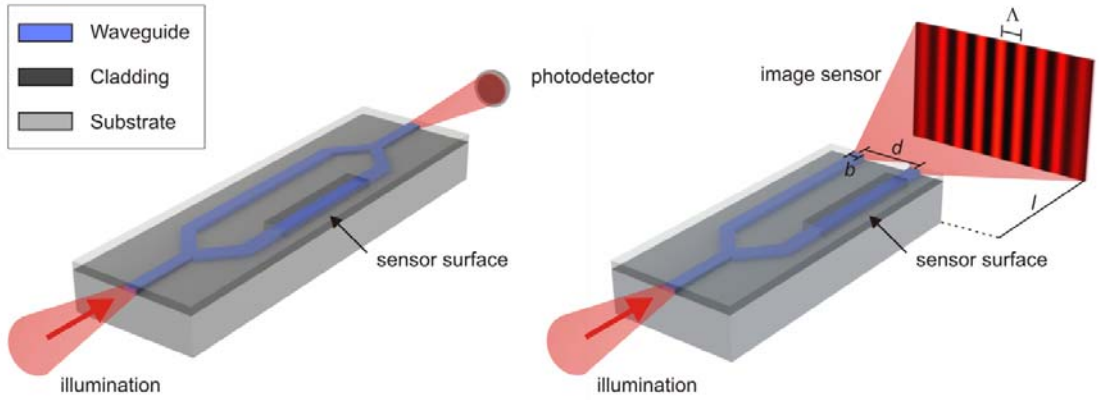

Figure 3: *Typical a) Mach-Zehnder and b) Young interferometer configurations.* The light coupled into the waveguide structure of the interferometer is split into two beams, which are passing through the sensor arm (and underneath the sensor surface) and the reference arm, respectively. In case of a Mach-Zehnder interferometer, the two beams are recombined by directing them to the same path again resulting in their interference. The beams of a Young interferometer are projected from two closely spaced secondary sources onto a detector array, where an interference pattern is detected. The spatial period of the fringes, Λ, the spacing of the two (secondary) sources, d, the distance of the plane of the sources and the detector surface, l, and the width of the slits, b, are also shown for the better understanding of eq. 3.3.

3.2. Wave propagation in Planar Optical Waveguides

The first demonstration of waveguiding is usually related to John Tyndall, however, Jean-Daniel Colladon has presented his "light fountain" earlier in 1842 (Colladon, 1842; Hecht, 1999). His experiment revealed that due to total internal reflection, the light can be guided in a transparent material, of which refractive index is higher than that of the surrounding ambient. This phenomenon has later been exhausted in many applications of the optical waveguides amongst others in telecommunication and sensor devices, in which the confinement and guidance of electromagnetic waves along an arbitrary but defined path in space is the basis of performance.

A group of optical waveguides, the so-called planar optical waveguides can be regarded as a byproduct of two industry branches, namely the telecommunication and semiconductor industries. Whereas the former led to novel methods to couple, transfer, switch, multi- and demultiplex light in optical fibers for high speed communication, the latter can be accounted for developing the technologies to master the fabrication of complex, miniature integrated optical systems on a wafer level (Anderson, 1965). In their simplest form, planar optical waveguides consist of a three-layer structure, in which a thin film (F) of thickness d_F is

sandwiched between a substrate (S) and a cover medium (C). The refractive indices of the layers are n_F, n_S and n_C, respectively. As it is depicted in Figure 4, light can be guided in the (waveguide) film by total internal reflection, if the refractive index of the film is higher than those of the surrounding media ($n_C < n_F > n_S$) and if the angle of light propagation relative to the interface normal is larger than the critical angles at the two boundaries ($\theta = \arcsin(n_{S,C} / n_F)$ based on Snell's law) (Jackson, 1998a). Nevertheless, waveguide modes can arise and propagate through the film without any loss of power (in ideal case, when no scattering and absorption occurs), if d_F is larger than a minimum or "cut-off" thickness, $d_{F\min}$, which is a function of the abovementioned waveguide parameters and the applied wavelength (Lukosz, 1995), and if the light rays reflected from the interfaces achieve constructive interference. As a consequence of the latter, only a discrete set of waveguiding states, i.e., of guided modes, exists in a planar waveguide configuration. This is the so-called self-consistency criterion of the classical "zig-zag" model interpretation (Saleh and Teich, 2007). It is important to note that if these constrains are not fulfilled, the guiding of the waves confined in the film cannot be performed and only radiation modes can be observed (Tien, 1977).

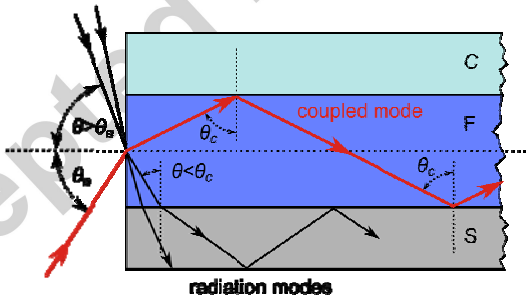

Figure 4: *Light propagation in a planar optical waveguide.* Light can be coupled and guided in a waveguide if $n_C < n_F > n_S$ and if the angle of light propagation relative to the interface normal is larger than the critical angle θ_c. Light entering the waveguide under an angle which is bigger than the acceptance angle θ_a, will lead to radiation modes and will be lost.

To get a deeper insight into this phenomenon, it is better to apply the Maxwell's equations and the proper boundary conditions to homogeneous, stationary, non-magnetic, source-free and nonconducting layers of a configuration written above. As it is discussed in Ref. (Jackson, 1998a), on the one hand, important consequences of the boundary conditions are not only

Snell's law and that the wave vector of original, refracted and reflected plane waves must lie in a plane, but also that the tangential component of a wave vector across an interface is continuous. This criterion defines a quantity, the effective refractive index $N = k_t / k_0$ for planar waveguides ($n_S, n_C < N < n_F$), where $k_t \equiv \beta$ is the tangential component of the wave vector, the so-called propagation constant. It reflects that N can be also introduced as $N = c_0 / v_{mode}$, where $v_{mode} = \omega / \beta$ is the phase velocity of the guided mode, c_0 is the speed of light in vacuum and ω is the angular frequency of the guided light. On the other hand, in case of planar waveguides, the plane wave solutions of Maxwell equations divide themselves into two orthogonal sets of functions. Modes with only two different polarizations can be excited; either the total electric or the total magnetic field is oscillating in the plane of the interfaces (Figure 5). These polarizations are denoted consequently as transversal electric (TE) and transversal magnetic (TM) modes, respectively (Saleh and Teich, 2007). Let us consider a general orthogonal coordinate system, where the modes are propagating along the z axis. Furthermore, the x and y axes are perpendicular and parallel to the interfaces, respectively. Based on the definition of TE and TM modes, we conclude that for $\underline{E}$ electric and $\underline{H}$ magnetic fields and consequently for the boundary conditions:

$$\text{TE: } E_x = 0,\ E_z = 0,\ H_y = 0,\ k_y = 0 \quad \text{thus} \quad E_y, H_z, \frac{\partial E_y}{\partial x} \quad \text{are continuous,} \tag{3.4a}$$

$$\text{TM: } E_y = 0,\ H_x = 0,\ H_z = 0,\ k_y = 0 \quad \text{thus} \quad E_z, H_y, \frac{\partial H_y}{\partial x} \quad \text{are continuous.} \tag{3.4b}$$

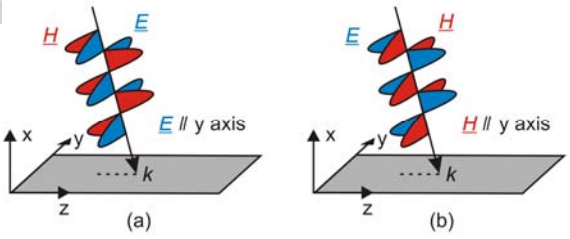

Figure 5: *Visualization of a.) TE and b.) TM modes.* In planar optical waveguides, modes with only two different polarizations can be excited; either the total electric or the total magnetic field is oscillating in the plane of the interfaces. These are the TE and TM modes, respectively.

Expressing Helmholtz wave equation (Jackson, 1998a) for these specificities, the following relationship can be revealed for the x component of the wave vector in the substrate, film and cover layers of a planar optical waveguide:

$$k_{x,X} = \pm k_0 \sqrt{n_X^2 - N^2}\,, \tag{3.5}$$

where X denotes S, F or C, respectively. In case of isotropic media, n_X is a single constant value and the solution of eq. 3.5 is independent from TE and TM polarizations. In case of anisotropic media, n_X is orientation dependent. Consequently, it is a matrix, which results in different solutions for TE and TM polarizations. A detailed description for anisotropy can be found in Ref. (Cottier, 2004; Kovacs et al., 2013). Corresponding to equation 3.5, the total electromagnetic field inside the wavguide film is given by the linear combination of an upwards, $\underline{U}^+(x,z,t)$, and a downwards, $\underline{U}^-(x,z,t)$, propagating wave:

$$\underline{U}(x,z,t) = \underline{U}^+(x,z,t) + \underline{U}^-(x,z,t) = \left(\underline{U}_0^+ e^{ik_x(x-x_0)+\varphi^+} + \underline{U}_0^- e^{-ik_x(x-x_0)+\varphi^-}\right) e^{iNk_0 z - i\omega t}, \tag{3.6}$$

where $\underline{U} = \underline{E}, \underline{H}$ and $\underline{U}_0 = \underline{E}_0, \underline{H}_0$. (It is visualized in Figure 6.) Considering eq. 3.5 and 3.6 it can be seen that the amplitude of the propagating waves attenuates exponentially outside of the waveguide film in the function of the distance measured from the nearest interface, since k_x becomes imaginary in the substrate as well as in the cover media. This exponentially decaying electromagnetic field is the so-called evanescent field. The penetration depth of the evanescent field (with other words the decay length of the field strength) can be gained by expressing eq. 3.5 and eq. 3.6 for the cover layer:

$$\delta_{x,C} = \left(k_0 \sqrt{N^2 - n_C^2}\right)^{-1}. \tag{3.7}$$

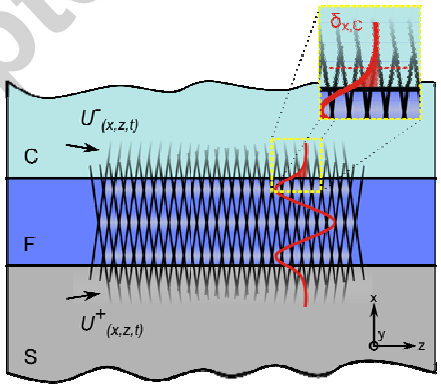

Figure 6: *Visualization of mode formation in a planar optical waveguide.* The total electromagnetic field inside the waveguide film is composed by the superposition of an upwards, $\underline{U}^+(x,z,t)$, and a downwards, $\underline{U}^-(x,z,t)$, propagating wave. Here, a mode of order 2 is depicted. The evanescent field with the penetration depth $\delta_{x,C}$ is magnified in the inset.

Applying eq. 3.6 at the film/substrate and film/cover interfaces, where $x = x_0$ and $x = x_0 + d_F$, respectively, the ratios of the upwards and downwards travelling waves can be written in the form of the (complex) Fresnel reflection coefficients r_S and r_C at the two interfaces:

$$r_S = \frac{\underline{U}_0^+}{\underline{U}_0^-} = |r_S| e^{i\varphi_S} \quad (x = x_0), \tag{3.8a}$$

$$r_C = \frac{\underline{U}_0^- e^{-ik_x d_F}}{\underline{U}_0^+ e^{ik_x d_F}} = |r_C| e^{i\varphi_C} \quad (x = x_0 + d_F), \tag{3.8b}$$

where φ_S and φ_C are phase shifts due to the reflection from the interfaces. The reflection coefficients can be expressed by the parameters of the waveguide, as well, as it is described in more detail in Ref. (Cottier, 2004). It is important to emphasize that they are different for TE and TM modes; consequently, TE and TM wave propagations can be performed under different conditions (also in case of isotropic media). Inserting eq. 3.8a into eq. 3.8b, the mode equation can be gained as:

$$r_S r_C e^{2ik_x d_F} = |r_S||r_C| e^{i(\varphi_S + \varphi_C + 2k_x d_F)} = 1, \tag{3.9}$$

which can be rewritten in order to conclude to the classical mode equation:

$$2d_F k_x - \varphi_S - \varphi_C = 2\pi m, \tag{3.10}$$

where m is the mode order. As it is demonstrated, due to the cross-sectional size and shape of the waveguide, only discrete electromagnetic field distributions characterized with N_m or β_m (see eq. 3.5) can be guided, because only these satisfy the boundary conditions. Figure 7 depicts the field-distribution profiles of the first four modes, i.e., TE_0, TM_0, TE_1 and TM_1 in planar optical waveguides. The number of modes of different orders is also determined by the opto-geometrical parameters. The orders are counted from zero referring to the shape of the wave fronts (Saleh and Teich, 2007). The number of guided modes decreases with d_F and refractive index contrast between film and surrounding or with increasing wavelengths. Waveguides not supporting any modes are below $d_{F\min}$ for a given wavelength, or vice-versa, a certain wavelength is below a distinct value determined by the cut-off frequency for a given waveguide configuration (Jackson, 1998b). In special case, when d_F is chosen to be slightly thicker than $d_{F\min}$, only the fundamental TE_0 and TM_0 modes can be excited and the waveguides are commonly called single-mode waveguides (Saleh and Teich, 2007). In a typical dielectric single-mode waveguide, d_F is about 100-200 nm.

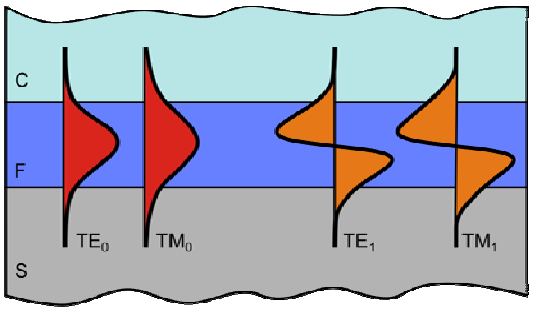

Figure 7: *Schematic visualization of the waveguide modes in a planar optical waveguide.* The field-distribution profile of the modes m=0 (red) and 1 (orange) for TE and TM polarizations are presented, respectively. As it is depicted, TM modes interrogate deeper into the surrounding media than TE modes.

3.3. Sensing with evanescent field

Depending on the waveguide configuration, mode, wavelength and polarization, the penetration depth and hence the sensitive region of the waveguide usually extends 30 – 150 nm into the cover medium, but it can be increased even up to about 1 μm using reverse symmetry waveguides (Horvath et al., 2005). Whereas in optical fiber communication, it may be regarded as a parasitic effect, since the optical power of the propagating mode can be decreased by scattering of the field at the boundary and/or by attenuation of the cladding, it allows waveguide sensors to investigate surface bound effects within the close proximity of the evanescent field.

As the evanescent electromagnetic field of the guided light penetrates slightly into the surrounding material, any refractive index change in the near-interface region has an effect on the value of *N*, in turn on the wavelength of the guided light causing a phase shift difference relative to an arbitrarily chosen original state:

$$\Delta\Phi = \frac{\partial\Phi}{\partial N}\frac{\partial N}{\partial n_c}\Delta n_c + \frac{\partial\Phi}{\partial N}\frac{\partial N}{\partial d_A}\Delta d_A = k_0 \cdot L \cdot S_c \cdot \Delta n_c + k_0 \cdot L \cdot S_A \cdot \Delta d_A, \qquad (3.11)$$

where L is the interaction length, $S_c = \partial N / \partial n_c$ and $S_A = \partial N / \partial d_A$ are sensitivities to cover refractive index n_C and adlayer thickness d_A changes, respectively. As it is discussed e.g. in Refs. (Guillod et al., 2013; Kunz and Cottier, 2006; Lukosz, 1995), a waveguide configuration can be optimized by means of fine tuning of the actual opto-geometrical parameters in order to maximize S_c and S_A. This flexibility of integrated optical waveguides

is a great advantage in (bio)sensor applications, since it gives additional degrees of freedom regarding choosing materials and designing structures (Lambeck, 2006).

In biosensor applications, not only n_C and d_A are the most important parameters, which are used to quantify an experiment. The adsorption of molecules onto the sensor surface is commonly described by mass per unit-area. The so-called surface mass density Γ of a protein adlayer can be determined by using De Feijter's formula:

$$\Gamma = d_A \frac{n_A - n_c}{\partial n / \partial c} , \tag{3.12}$$

where n_A is the adlayer refractive index and $\partial n / \partial c$ is the derivative of solution refractive index with respect to protein concentration (De Feijter et al., 1978).

Particularly changes in the optical properties of the cover are of interest and can directly be translated in either bulk refractive index changes in refractometry measurements or mass loading on the waveguide surface by the adsorption of e.g. biomolecules in biosensoric investigations. Since a real sensor configuration is affected by measurement noise, it is practical to characterize its sensing capabilities with its detection limit (or limit of detection) for bulk refractive index and/or surface mass density changes. The detection limit is the lowest change of a parameter that can be detected within a stated confidence limit. Its value is calculated simply by the multiplication of a confidence factor (f_c , generally chosen to be 3 in biosensorics) and a ratio of noise in the transduction signal, σ , and the response of the configuration for a unit change of the measured parameter, s (Long and Winefordner, 1983):

$$LOD = f_c \frac{\sigma}{s} . \tag{3.13}$$

The quantification of different configurations with their limit of detection allows for a comparison in a simple and objective manner.

3.4. Waveguide types and light coupling techniques

Planar optical waveguides exist in various configurations differing in both material as well as geometry, since their technology offers a great flexibility and variability in sensor design, production and optimization (Lambeck, 2006). Generally, planar waveguides deposited on a stable and thin substrate, which is typically made of low refractive index and glassy materials (e.g. SiO_2 or polymers), can be classified into two types regarding their geometrical design, namely slab waveguides and channel waveguides (Campbell, 2008). It is important to note that the theory of planar optical waveguides introduced in the previous sub-chapter is exact

for slab waveguide modes and is a very good approximation for channel ones (Lambeck, 2006). Slab waveguides are structures with a planar geometry, which guide light in only one transverse direction as lateral modes become effectively infinite (Snyder and Love, 1983). Despite the relatively easy fabrication, another benefit of the slab waveguide is the absence of scattering between the transverse and lateral modes. Contrary to the slab waveguides, channel waveguides act as a conduit for the light in both transverse directions with a two dimensional optical confinement. Channel waveguides can be further divided into buried channel, strip-loaded, diffused, ridge and rib waveguides (Figure 8) and are microfabricated by embossing or conventional photolithographic means (Anderson, 1965). A buried waveguide is embedded in the substrate and completely surrounded by the cladding material and therefore not a suitable configuration for the sensitive area of the interferometer, but it is commonly used to guide the light from and to the latter. Another method to form a waveguiding channel is to load a dielectric strip on top of a slab waveguide. This induces a localized difference in the underlying effective refractive index and is known as strip-loaded waveguide. Again, due to the shielding cover cladding, this configuration is not beneficial for biosensing applications. A third method to form a laterally confined waveguide is the diffused waveguide, which is formed by indiffusion of foreign atoms or by ion exchange. In the field of planar optical interferometric waveguide biosensors, the ridge and the rib waveguides are the most common of their kind, whereas the former is a fully, the latter a partly freestanding channel structure on top of a supporting substrate. An alternative rib waveguide configuration is the anti-resonant reflecting optical waveguide (ARROW) fabricated with standard integrated circuit technology (Benaissa and Nathan, 1998; Duguay et al., 1986; Jiménez et al., 1996). In an ARROW waveguide, the light is confined in a waveguide rib, which is separated from a semiconductor substrate with two interference layers. The light confinement is based on total internal reflection at the ambient-waveguide film interface and on high anti-resonant reflection (>99.9%) from the interference cladding layers. The interference layers behave as a Fabry-Perot resonator, consequently, single-mode behavior is guaranteed by loss discrimination. The advantages over the conventional total internal reflection waveguides include the greater film thickness, the greater freedom regarding their fabrication parameters and the lower insertion losses (Prieto et al., 2000).

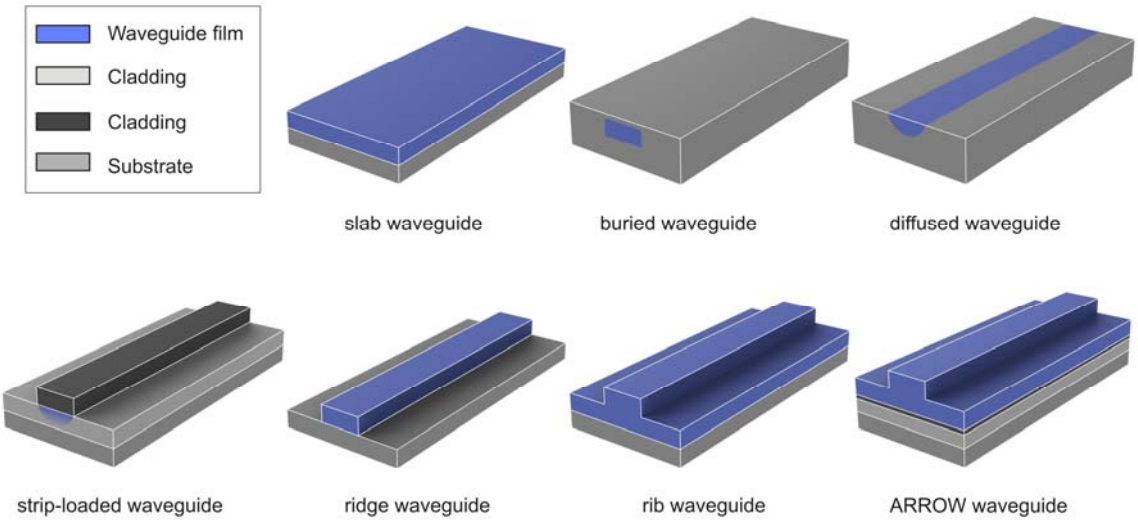

Figure 8: *Schematic 3-dimensional representation of different waveguide types*. In the interest of an easier comparison, the same functional layers are marked with same colors (see the inset in the upper left corner).

Depending on their refractive index profiles, both categories can be divided into three sub-groups, namely step-index, graded-index and photonic crystal waveguides. Step-index waveguides exhibit an abrupt refractive index step at the substrate-waveguide and cover-waveguide transitions. Most commonly, a thin layer of a high refractive index material (e.g. Ta_2O_5, TiO_2, Si_3N_4, Al_2O_3 or SiON) is deposited on the substrate (Brecht and Gauglitz, 1995). In the case of a graded-index waveguide, the refractive index profile has a smooth transition between cover and substrate as they are fabricated by diffusive ion-exchange or more recently, written in glass by femtosecond laser pulses (Chen et al., 2007; Davis et al., 1996). Contrary to step-index waveguides, only rather small refractive index contrasts can be achieved for graded-index waveguides and therefore exhibit a lower sensitivity (Parriaux and Veldhuis, 1998). Step-index and graded-index waveguides are depicted in Figure 9. Photonic crystal waveguides are composed of repetitive regions of low and high dielectric constants that affect the propagation of the electromagnetic waves by diffraction and interference effects (Joannopoulos et al., 2008), but they are out of the scope of the present review.

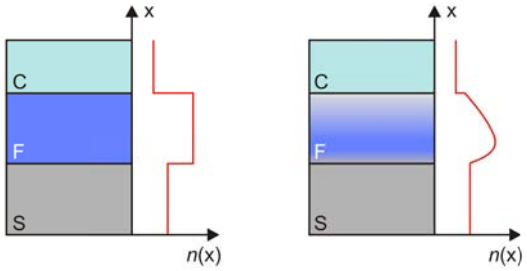

Figure 9: *Step-index and graded-index waveguides*. Step-index waveguides exhibit an abrupt refractive index step at the substrate and cover transitions, while the refractive index profile of graded-index waveguides has a smooth transition between them.

In waveguide applications, light from an external source needs first to be coupled into and subsequently out of the waveguide for detection. In general, five coupling methods can be differentiated as follows: free-space end-fire-, butt-end-, prism-, grating- and directional coupling (Figure 10). The reader is referred to specialized books for further literature on this topic (Saleh and Teich, 2007; Tamir, 1975).

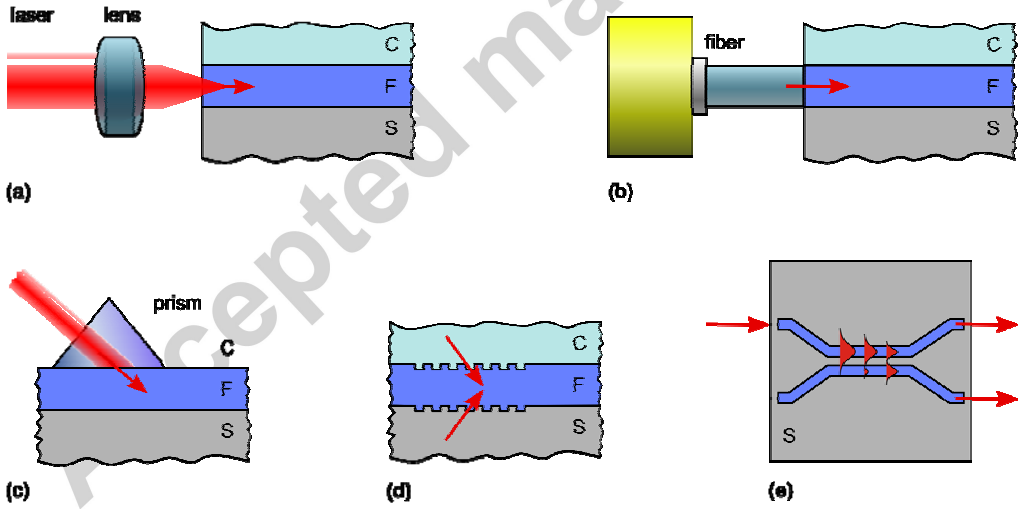

Figure 10: *Light coupling techniques for optical waveguides:* (a) end-fire coupling, (b) butt-end coupling, (c) prism coupling, (d) grating coupling and (e) directional coupling.

In the case of free-space end-fire coupling, the illumination light is directly focused on a cleaved edge face of the waveguide. It can be regarded as the most common and simplest way to couple a free-space source into a waveguide. However, for efficient coupling, the end faces must be extremely smooth and the numerical aperture of the focusing lens needs to be fitted to

the propagation constant of the mode excited in the waveguide film. Moreover, the precise alignment of the impinging beam relative to the waveguide is of crucial importance for high coupling efficiency and makes high demands on the positioning devices and their mechanical stability, especially for thin single-mode waveguides.

The closely related concept of butt-end coupling brings an optical fiber in direct contact (often via immersion oil) with the cleaved edge face of the waveguide. Advantageous is the fact that two physical units need to be aligned and brought in contact, which is generally easier than the alignment of a light cone (especially for wavelengths beyond the visible spectrum) and can be done under a microscope or even with fiber guiding alignment grooves. Similarly to end-fire coupling, the alignment is crucial as well as the mode matching between the two waveguides for the efficient coupling. Further difficulties of the butt-end approach are the the presence of immersion oil (if applied) and the fact, analogue to the chicken or the egg problem, that the light already needs to be coupled in the optical fiber.

A third method to couple light into a waveguide is via prism coupling (Osterberg and Smith, 1964). A high refractive index prism is either brought in direct contact with the waveguide by applying mechanical pressure or by the use of immersion oil. Illuminating the waveguide through the prism at an incident angle that matches the propagation constant of a guided mode, light can be coupled into but also extracted from the waveguide with high efficiency. The need for mechanical pressure or immersion oil and the direct contact of the prisms with the waveguide make these couplers unfavorable for sensing applications. In practice, this is because the applied pressure can lead to slight waveguide deformations, whereas the immersion oil may contaminate the waveguide surface. Additionally, the prism's physical size is disadvantageous in bioexperiments, since prism and flow-cell need to be mounted on the same side of the waveguide.

Waveguide grating couplers are periodic structures with an alternating effective refractive index, usually with a grating period in the range of lambda half of the coupled light (Dakss et al., 1970; Peng et al., 1975; Tamir and Peng, 1977). The grating either consists of a periodically corrugated surface relief, realized by embossing or photolithographic processes or an alternating modification of the waveguide refractive index. The latter can either be achieved persistently by ion exchange or UV induced refractive index modulation (Hamori and Nagy, 2004). In general, both the coupling of an impinging coherent beam and conversion into a guided mode within the waveguide, as well as the reciprocal process of coupling the light out of the waveguide by means of grating couplers is defined by the resonance condition:

$$n_0 \sin \alpha_l = \frac{\lambda_{fs}}{\Lambda} l - N \tag{3.14}$$

where α is the coupling angle, l is the diffraction order, λ_{fs} is the wavelength measured in free-space and Λ is the grating period. The grating acts as a diffractive element to achieve higher order diffraction angles within the waveguide, which fulfill the TIR conditions. Waveguide grating couplers offer various advantages compared to the abovementioned methods: First, free space coupling into the expanded grating elements is rather easy, as only the coupling angle of a collimated beam needs to be adjusted. Second, contrary to the prism coupler, light can be coupled via both sides, via the substrate or the cover, of the waveguide. Since the fluidic chamber for the sample analysis is placed on the cover side of the waveguide sensor, hereby obstructing the light, coupling via the substrate is commonly applied. Additionally, no immersion oil is needed. As drawbacks, it has to be mentioned that the production of waveguide gratings is technology-intensive and they are also sensitive for mechanical vibrations, since the coupling efficiency is very sensitive function of angle of incidence (Vörös et al., 2002).

In the case of directional coupling, channel waveguides are brought in close proximity, so that a mode can be excited in a secondary waveguide via the evanescent filed of a primary one (Marcatili, 1969). In other words, one of the two waveguides acts as the source for the second one, whereby the amount of optical power transfer from the former to the latter can be adjusted by geometrical means like interaction length and their relative distance. The concept of directional coupling is mainly used for signal multiplexing or coupling into ring resonators, where this sophisticated and stable coupling mechanism is necessary, but it has the disadvantage that their production is technology-intensive and, analogue to the butt-end coupling, the light already needs to be coupled into one of the waveguides beforehand.

4. Integrated Planar Optical Waveguide Interferometers

Usually, the integrated planar optical waveguide interferometers are classified solely based on their configurations into numerous groups, such as Mach-Zehnder-, Young-, Hartman-, dual polarization-, bimodal waveguide interferometry, etc. without explaining the connections among them (Duval et al., 2012a; Estevez et al., 2012; Fan et al., 2008; Lambeck, 2006). However, a more strict classification based on the theoretical background summarized above would give a more relevant and brighter overview of the system of the individual sensors.

Discussing the waveguide interferometers in this way, the connections among the individual methods, the common advantages and disadvantages of the groups can easily be revealed and summarized. This review classifies the waveguide interferometers in a manner focusing first onto their basic sensor scheme, such as common- and double path interferometers, regarding whether the beams, which later produce the interference response signal, are propagating on the same or on different paths. After this separation, they are distinguished by their basic working principle, namely, whether the detection mechanism is based on intensity measurement (Mach-Zehnder interferometer) or on the monitoring of an interference pattern (Young interferometer). The subchapters try to follow a chronological order to illustrate the evolution of the field of waveguide interferometer biosensors.

In a double path waveguide interferometer, waveguide modes of the same order and polarization are propagating through two laterally separated waveguide channels, while they interact with different samples at different sensing regions resulting in their relative phase shift. (The reference arm can be also hidden from the environment.) At the same time, this working principle can be extended to common path waveguide interferometers in a way that the modes are propagating on the same path, but they either have perpendicular polarizations or they are representing different mode orders. Passing through the sensing region the two modes undergo different phase shifts due to the different sensitivities valid for different polarizations or orders (Gut, 2012). As it can be seen in the followings, the application of Mach-Zehnder or Young interferomtery does not depend on whether the interferometer has one or two paths.

4.1. Common Path Waveguide Interferometers

The first publication of common path waveguide interferometer is related to Hartman et al. in 1988 (Hartman et al., 1988). The technique was elaborated by Lukosz and Stamm, who have presented a Mach-Zehnder-type integrated optical *difference interferometer* as relative humidity sensor in 1991 (Lukosz and Stamm, 1991). Their setup is based on a monomode planar waveguide, into which the light originated from a coherent laser source is end-coupled exciting TE_0 and TM_0 modes. Although both modes propagate on the same path and interact with the same sample on the same waveguide section, the total phase shifts of the two polarizations induced by a change of the sample over the sensing region are not equal, since the sensitivities of the modes are different for a refractive index change performed above the sensing region. This results in turn in different phase shifts (see eq. 3.11) (Lukosz, 1991).

Combining the two modes into an interference intensity signal and recording its variation in time, the changes of the sample can be detected as a time-dependent phase difference:

$$\Delta\Phi(t) \equiv \Delta\Phi_{TE_0}(t) - \Delta\Phi_{TM_0}(t) = 2\pi(L/\lambda)\left[\Delta N_{TE_0}(t) - \Delta N_{TM_0}(t)\right], \tag{4.1}$$

where t is the measurement time. Three methods have been reported to measure the interferometer's response (Lukosz, 1995; Lukosz et al., 1997). The first setup (see Figure 11a), which is called 'original' by the authors, comprises a lens to parallelize the light coupled out through the end-edge of the waveguide, a beam splitter and two Wollaston prisms to effect the interference of the polarizations on the surface of four detectors. Furthermore, a half-wave ($\lambda/2$) plate and a quarter-wave ($\lambda/4$) plate were also installed into the setup in order to record four interference intensity signals (i=1…4) with different additional phase shifts of 0, π/2, π and 3π/2, simultaneously:

$$I_i(t) = \frac{I_{A,i}}{2}\left\{1 + \cos\left[\Delta\Phi(t) + (i-1)\frac{\pi}{2} + \Delta\Phi_0\right]\right\} + I_{B,i}, \tag{4.2}$$

where $I_{A,i}$ and $I_{B,i}$ are the amplitude of signal intensity variation (AC signal) and the constant background intensity (DC signal), respectively, measured with the ith detector, $\Delta\Phi_0$ is a constant phase value measured at t=0. The phase determination based on four-point measurement has a clear advantage over single-point measurements. If the sensitivity for phase difference disappears at the constructive and destructive interference points, the two signals recorded with the other two detectors (1, 3 or 2, 4) compensate the problem, since they are in this case at the quadrature points with maximum sensitivity. However, while the phase turns around, the sensitivity oscillates between a maximum and a minimum value. The time-dependent phase difference relative to an arbitrary initial value was determined for the interval $-\pi$ to π applying the following relation:

$$\Delta\Phi(t) + \Delta\Phi_0 = \arctan\left\{\frac{\left[I_1(t) + I_2(t)\right]\left[I_3(t) - I_4(t)\right]}{\left[I_1(t) - I_2(t)\right]\left[I_3(t) + I_4(t)\right]}\right\} \tag{4.3}$$

and the sign of $\left[I_1(t) - I_2(t)\right]$ or $\left[I_3(t) - I_4(t)\right]$. Combining the intensity values in this way, the effect of laser power fluctuations and changes of the attenuation of the guided modes can be minimized, thus an improved signal-to-noise ratio of the response signal can be obtained. Stamm and Lukosz have reported about an experimental phase resolution of $\Delta\Phi_{\min} = 5\times10^{-4}\times2\pi$ rad and a detection limit of 2×10^{-7} and 0.13 pg/mm^2 for bulk refractive index and surface mass density changes, respectively, at the wavelength λ =632.8 nm (Stamm and Lukosz, 1994, 1993).

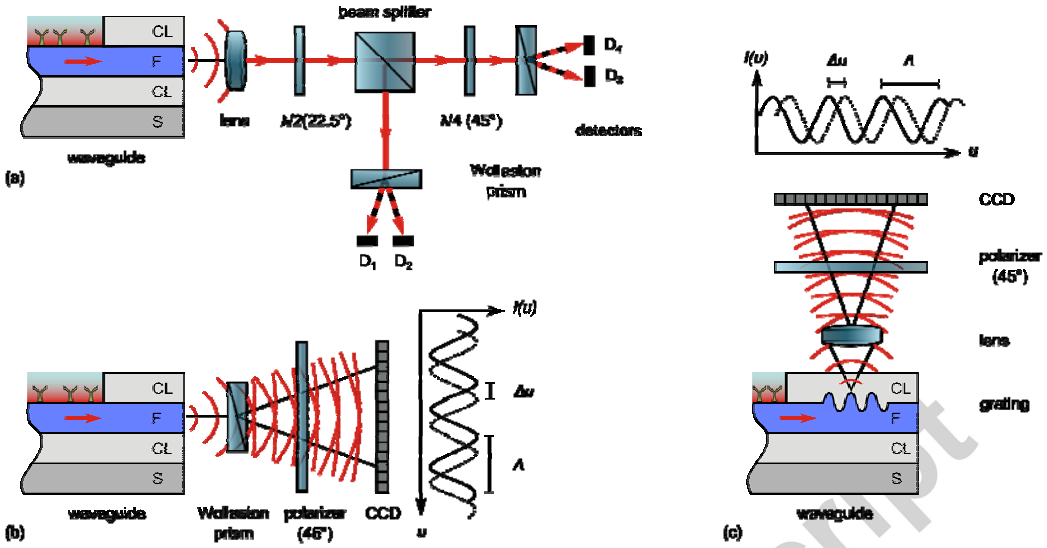

Figure 11: *The three difference interferometer of Lukosz and Stamm*. The configuration and working principle of a) the 'original' Mach-Zehnder interferometry-based difference interferometer as well as b-c) the second and third version developed later based on the principle of Young interferometry are depicted in the images, which are redrawn based on Ref. (Lukosz et al., 1997).

To attempt to improve the $\Delta\Phi(t)$ and ΔN resolution, Lukosz's group has proposed two other methods for the measurement of the time-dependent phase difference in 1997, which overcome the problem of sensitivity fading and the intensity calibration (Lukosz et al., 1997). Both of their setups were based on Young interferometry implementing the work of Nakadate (Nakadate, 1990, 1988). These two alternative methods can be seen in Figure 11 and their working principle can be briefly summarized as follows: After passing through a polarizer, the divergently propagating TE_0 and TM_0 modes are combined into a spatial interferogram, which is recorded with a linear detector array. The interferograms are evaluated using fast Fourier transform, which permits to determine the total phase difference, in turn the total lateral shift $\Delta u(t)$ of the interference fringes and the difference of the effective refractive index changes over the sensing region:

$$\Delta N_{TE_0}(t) - \Delta N_{TM_0}(t) = \left(\frac{\lambda}{L\Lambda}\right)\Delta u(t) = \left(\frac{\lambda}{2\pi L}\right)\Delta\Phi(t). \qquad (4.4)$$

To distinguish between the two methods, it should be mentioned that they are designed for different outcoupling techniques. In case of an end-fire coupling, a Wollaston prism takes part in the interferogram formation and in case of a surface relief grating coupling, a lens is placed in front of the polarizer. Although, these methods are not more sensitive compared to the

original one, they comprise fewer expensive optical elements, thus they can be built cheaper in a smaller size. Consequently, an extension to multi-channel measurements is more straightforward (Lukosz et al., 1997). Furthermore, the original four-point measurement contains insufficient information for a self-calibration, which can lead to phase-uncertainty in case of improper calibration values or changed system parameters. The spatial interferogram gives rise, however, to overcome this problem.

In addition to humidity sensor applications, the difference interferometer was also used as refractometer and biochemical sensor. Huber et al. have published the first immonosensing measurements in a detection limit comparison study of surface plasmon resonance, input grating coupler and difference interferometer (Huber et al., 1992). Schlatter et al. have presented the difference interferometer as a direct affinity sensor (Schlatter et al., 1993). Simultaneously, Stamm et al. have demonstrated the sensing capabilities in refractometry measurements (Stamm and Lukosz, 1993). An important work also from Stamm et al. is a difference interferometer operating simultaneously at two laser wavelength (λ_1=632.8 nm, λ_2=488 or 491 nm). As it was demonstrated in Ref. (Stamm et al., 1998), the dual-wavelength operation allows to differentiate the bio-specific interactions from temperature fluctuations or refractive index variations of the sample solution.

The difference interferometer is a momentous configuration, not only since it is probably the first integrated planar optical waveguide interferometer biosensor. Its sensing capabilities are also remarkable even compared to today's sensors (see the following sections). Focusing on the disadvantages, it has to be mentioned that the difference interferometer sacrifices the information, which could be revealed from the independent TE and TM modes, in order to gain a lower detection limit of the changes over the surface region. Furthermore, a fully integrated difference interferometer is not easily realizable due to the robust and not easily integrable parts applied in the presented setups. The end-fire coupling to excite the modes and the detection based on the interference pattern created off-chip (in the second and third version of difference interferometer) requires high mechanical stability of the device, which can lead to lower ability in point-of-care applications.

Although the difference interferometer is a great and original work, it has never been in the limelight. Its development was performed slowly and only a few studies have been reported by other groups; e.g. a sensor was constructed using prism couplers (Tsunoda et al., 1999), the idea was implemented into the field of surface plasmon resonance spectroscopy (Debackere et al., 2006) and a theoretical and comparative analysis was also presented (Levy and Ruschin,

2009). In the last years, however, a new version of the difference interferometer, the so-called *bimodal waveguide interferometer* has been developed by Zinoviev et al. (Zinoviev et al., 2008, 2011). The basis of this integrated biosensor is also the interference of two waveguided modes propagating in a common path interferometer. However, the TE_0 and TE_1 modes are indirectly excited in this case. The light of a coherent source is coupled into a ridge waveguide, which is supporting only a single TE mode. Through a modal splitter, namely through a vertically asymmetric junction, this mode is coupled into another waveguide, which allows two transversal modes to propagate. Consequently, the fundamental mode of the first waveguide excites not only TE_0, but TE_1 as well. The modes are propagating under the sensing region towards the end facet of the waveguide, where they are coupled out creating an intensity pattern on the surface of an off-chip two-sectional photodetector and the shift of the intensity maximum is detected, which can be related in turn to the effective refractive index changes at the sensing region (Figure 12). The sensing capabilities of this setup are similar compared to the difference interferometer; a phase resolution limit of $5\times10^{-4}\times2\pi$ rad and a detection limit of 2.5×10^{-7} for bulk refractive index changes have been presented, which corresponds to a detection limit of about 0.05 pg/mm^2 for surface mass density changes. As a continuation of this work, Duval et al. have recently published a more sophisticated bimodal waveguide interferometer design supported with microfluidics, which makes a 4×4 channel measurement on a 30×10 mm^2 sensor chip possible with similar resolution (Duval et al., 2012b). Setting aside the common drawbacks peculiar to the working principle (see the previous paragraph), the advantages of this system compared to the difference interferometer are that it does not need any additional polarizer or Wollaston prism to effect the interference of the two modes, which in turn can lead to a more compact design. Furthermore, a higher sensitivity can theoretically be achieved based on the interference of modes of the same types instead of the same orders (Gut, 2012). The miniaturized multi-channel sensor chip makes the interferometer promising for point-of-care applications.

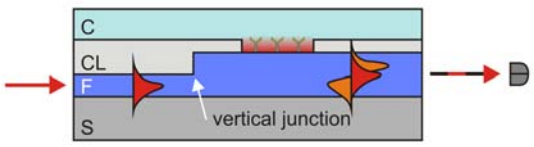

Figure 12: *Bimodal waveguide interferometer.* Through a vertically asymmetric junction, i.e., a modal splitter, the fundamental mode excites both TE_0 and TE_1 modes. After propagating through the waveguide underneath the

sensor surface towards its end facet, both modes are coupled out creating an intensity pattern detected by a two-sectional photodetector.

Based on the work of Tiefenthaler and Lukosz in 1984, it is well known that waveguide gratings cannot only be used as integrated optical elements to facilitate the coupling into and out of the waveguide, but they can also act as very sensitive transducers themselves (Tiefenthaler and Lukosz, 1988, 1984). The literature on waveguide grating couplers, their application as label-free biosensors and various interrogation schemes is vast and out of the scope of this review. Nonetheless, the *bidiffractive grating coupler* with its interferometric readout principle as it was introduced by Fattinger in 1995 belongs to the class of common path waveguide interferometers (Fattinger et al., 1995). Following eq. 3.13, it is obvious that any change in the waveguide's effective refractive index of a given device causes a change in the coupling angle at a given wavelength. This underlying principle is the basis of the bidiffractive grating coupler, which consists of a planar slab waveguide with two incorporated, superimposed uniform microrelief gratings with different periodicity and/or orientation (see Figure 12). Since the frequency spectrum of the bidiffractive grating consists of two fundamental spatial harmonics, two distinct resonance angles are simultaneously present for a given mode. This key feature allows a distinct, background-free separation of the reflection and transmission of the incident beam and the outcoupled beam (Fattinger, 1993). The waveguide is supporting only the two fundamental modes TE_0 and TM_0. By adjusting the two grating constants, the corresponding coupling angles for the two modes can be set independently from each other. In particular, they can be set to a selected angular position and a pre-defined angular separation. Impinging the two incoupling beams at the same lateral position, the angular separation of the outcoupled beams from the two modes can be directly monitored by a detector array or position sensitive device. Instead of only monitoring the angular positions of the two outcoupled beams, the distinct overlap of the outcoupled beams of the bidiffractive grating coupler allows a differential interferometric read-out of the angular separation of the two beams by placing a polarizer at 45° in front of the detector array (diode array, CCD or CMOS array), hereby forming an interference pattern on the latter. Since the sensitivity and hence the angular change upon an effective refractive index change differ for the two modes, the spacing of the fringes in the interference pattern changes. Performing the Fourier-transformation of the fringe pattern, the shift of its spatial frequency can directly be related to the change of the transducer's response on changes of the refractive index (Fattinger et al., 1995).

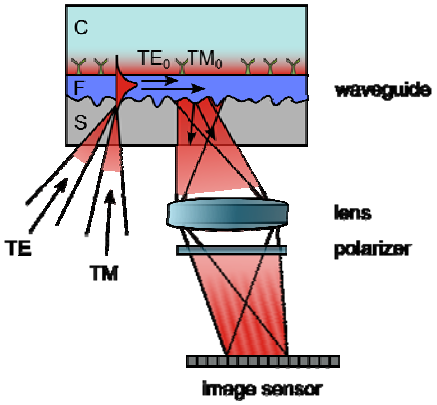

Figure 13: *The bidiffractive grating coupler.* This configuration allows coupling in the waveguide at well separated angles for the TE and TM modes, respectively, but common outcoupling angles due to the superimposed gratings. The overlapping beams form an interference pattern which can be monitored by an image sensor. The image is redrawn based on Ref. (Spinke et al., 1997).

The first application of bidiffractive grating coupler for biosensing, namely for direct immunosensing, was published by Spinke et al., who revealed a detection limit of about 24 pg/mm^2 for surface mass density changes (Spinke et al., 1997). By further development of the sensor, this value was improved by O'Brien et al. to 6 pg/mm^2 measured also in immunoassay experiments (O'Brien et al., 2000).

One of the main advantages of the bidiffractice grating coupler certainly is its position-insensitive coupling principle, making it an appealing candidate for array based, multiplexed sensor systems. Additionally, the differential sensing scheme eliminates, in the first order, adverse mechanical as well as thermooptical effects. On the other hand, the need for an overlap of the two outcoupled beams poses high requirements regarding the precision and uniformity of the waveguide thickness and its gratings.

4.2. Double Path Waveguide Interferometers

Obviously, the most important advantages of common path waveguide interferometry over double path waveguide interferometry are rooted in the fact that the modes are propagating on the same path. On the one hand, it results usually in smaller sensitivity to environmental noise, since the paths are not separated in space. Therefore, the noise affects the modes similarly and in turn appears in the phase difference dependent response signal only weakly. On the other hand, the common path waveguide interferometer configurations are relatively simple; their production is cheaper and easier, because complex surface processing is

needless. Additionally, multi-channel measurements applying them have also better perspectives, since in theory, twice as many sensing window can be placed on the same area. Nevertheless, the application of only one beam makes the setup in the same way disadvantageous, as well. Any change of the sample on the sensing window shifts the phases of both modes simultaneously and with different magnitudes, but in the same direction. Accordingly, the sensor's response is smaller, since the phase difference of the modes are significantly smaller compared to the case, if stationery phase reference is applied. An additional important drawback is that the common path waveguide interferometers lack the inherent possibility of referencing, which is a typical characteristic of fully integrated double path waveguide interferometers. Consequently, the differentiation between the binding of target molecules and unspecific adsorptions or a refractive index change of the cover medium is difficult in single-channel measurements. Moreover, they utilize typically additional optical parts to combine the modes into an interference pattern. These arguments pro and contra expose why researchers have developed side-by-side biosensors of common as well as double path configurations and which limitations they tried to overcome in the meanwhile. The following chapter summarizes the most important milestones of double path waveguide interferometers divided into three subgroups, such as conventional Mach-Zehnder, phase modulated Mach-Zehnder and Young interferometers, respectively.

4.2.1. Conventional Mach-Zehnder interferometers

The double path Mach-Zehnder interferometers are well-suited both as fully integrated as well as hybrid optical sensors. A typical fully integrated implementation comprises two Y-junctions in single-mode waveguide layer. One of them splits the guided mode into the sensor and reference arms, while the other recombines the arms after a certain distance. The waveguide film is covered with a cladding layer apart from a section above the sensor arm, where the guided mode interacts with the sample over a length L. The light is typically coupled into the interferometer by end-fire coupling or by grating relief coupling. The hybrid Mach-Zehnder interferometers are partially integrated sensors, which means that the splitting and the recombination of the beams are done off-chip by applying conventional optical elements. Accordingly, a higher response for mechanical vibrations characterizes the hybrid Mach-Zehnder interferometers, while relatively high fabrication costs due to the complex surface structure are typical for the fully integrated ones. Since the theory behind the working principle of every Mach-Zehnder interferometer is the superposition of two coherent plane

waves (modes) with different phases, eq. 4.1 and eq. 4.2, which describe the output signal of difference interferometer, can be rewritten in a compact form as:

$$I(t) = \frac{I_A}{2}\left\{1 + \cos\left[2\pi\frac{L}{\lambda}(N_S(t) - N_R(t)) + \Delta\Phi_0\right]\right\} + I_B, \quad (4.5)$$

where $N_S(t)$ and $N_R(t)$ are the effective refractive index values measured at the sensor and reference arm, respectively.

The first publications of hybrid and fully integrated Mach-Zehnder interferometers for biosensor applications could be found in the literature in the early 90's already. Heideman et al. presented a two-channel hybrid interferometer setup in 1991 (see Figure 14a), in which the beam splitting and recombination is performed by two cubic beam-slitters and the beams are coupled into the chip and out of it using surface relief gratings (Heideman et al., 1991). The capabilities of this sensor have been presented in immunosensing measurements and it was demonstrated that a minimal phase change of $1\times10^{-2}\times2\pi$ rad can be unambiguously detected, which corresponds to a bulk refractive index change of 4×10^{-6} (Heideman et al., 1993). (The continuation of this work can be found in the next subchapter.) An early application of a fully integrated Mach-Zehnder interferometer for biosensing has been published by Ingenhoff et al. in 1993 (Ingenhoff et al., 1993). The working principle of their configuration is based on applying two Y-junctions and end-fire coupling as it is written in the previous paragraph and depicted in Figure 14b. Their research was directly continued by Prieto et al. for example, who presented an improved integrated optical design with a detection limit of 7×10^{-6} for bulk refractive index changes (Prieto et al., 2003a). The same group proposed also a similar configuration based on ARROW technology for biosensing. Although ARROW structures are advantageous regarding core thickness, insertion losses and mass production, they are typically accompanied by lower detection limit. Prieto et al. revealed also a lower value of 2×10^{-5} for bulk refractive index changes with their ARROW based biosensor (Prieto et al., 2003b).

Meanwhile, slightly modified configurations have also been reported. By means of a third Y-junction, Brosinger et al. introduced a third waveguide in order to reference the intensity fluctuations of the coupled light. Furthermore, they opened the cladding layer over the reference arm as well, forming a reference sensing area and coated the sensor area with recognition elements and blocked both of the areas in order to compensate the unspecific affinity bindings. They demonstrated a detection limit of 2×10^{-5} for bulk refractive index

changes (Brosinger et al., 1997). This work was continued later by Weisse et al. and Busse et al. (Busse et al., 2001; Weisser et al., 1999), for example. A similar, but less sensitive configuration has been reported by Schipper et al. (Schipper et al., 1997). Drapp et al. have presented a modified Mach-Zehnder interferometer, which incorporates a three-output directional coupler (Figure 14c). Instead of applying a second Y-junction for the beam recombination, mode coupling is used in this case to exchange power from the reference and sensor arms between the three outputs of the coupler. The main advantages of this modified system are based on the simultaneous detection of three response signals shifted in phase with $2\pi/3$. This detection principle makes a significant decrease of sensitivity fading possible in order to cancel out the effects of intensity fluctuations. With this setup, the authors could perform unambiguous detection with a detection limit of 1.5×10^{-6} for bulk refractive index changes (Drapp et al., 1997). The theoretical description of the operation can be found in Ref. (Luff et al., 1998). Further improvements were later proposed by Hua et al. (Hua et al., 2002).

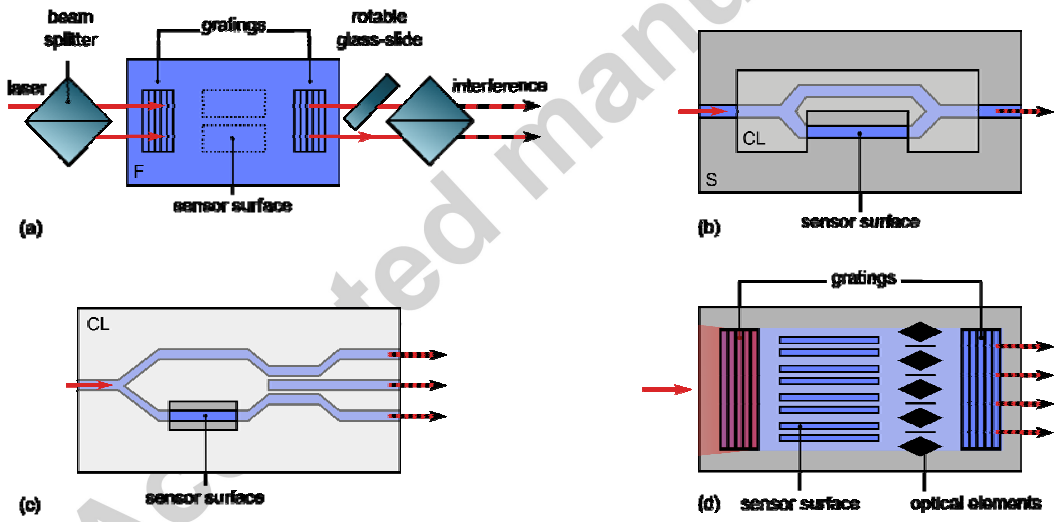

Figure 14: *Double path Mach-Zehnder interferometers.* The configuration and the working principle of a) the hybrid interferometer of Heidemann et al., the fully integrated interferometer of b) Ingenhoff et al. and c) Drapp et al. and d) the Hartman interferometer are schematically presented. The images are redrawn based on Refs. (Drapp et al., 1997; Hartman et al., 1995; Heideman et al., 1993; Ingenhoff et al., 1993).

A typical drawback of fully integrated Mach-Zehnder interferometers is the complexity of their sensor surface, which makes the chip fabrication more technology- and cost-intensive compared to that of simple planar waveguide sensors, such as e.g. difference interferometers or hybrid Mach-Zehnder interferometers. An early endeavor to simplify the sensor surface is related to Hartman et al. (Hartman et al., 1995), who have published an integrated Mach-

Zehnder interferometer based on planar waveguide in 1995. As it was demonstrated, in a so-called *Hartman interferometer*, a broad beam of parallel and coherent light is coupled into the waveguide chip through a broad input grating, then it propagates parallel to and under multiple sensing regions of the waveguiding film. After this section, integrated optical elements are placed to combine the light passing through the adjacent regions resulting in interference signals. The interference signals of the paired strips, which are characterizing the procedures performed on the sensor arms relatively to the reference arms are outcoupled by a broad output grating and detected with photodiodes (Figure 14d). In two channel measurements, first Hartman et al., later Schneider et al. have demonstrated the sensor capabilities in biological experiments of pathogen, nucleic acid and protein detection (Hartman et al., 1995; Schneider et al., 1997). A few years later, two reports were published on immunosensing applications (Schneider et al., 2000a, 2000b). Limit of detection of bulk refractive index or surface mass density changes were not documented for the original configuration. In fact, this sensor configuration has not solved the problem of sensor surface complexity, moreover, the sensitivity fading and directional ambiguity is also a characteristic of this approach. Consequently, the concept could not spread world-wide.

4.2.2. Phase modulated Mach-Zehnder interferometers

The most important and common disadvantages of the hybrid and fully integrated Mach-Zehnder interferometers mentioned in the previous subchapter is the sensitivity fading similarly to that detailed in the case of 'original' difference interferometer. Furthermore, in several configurations, the effect of the intensity fluctuations due to light source and coupling instabilities and the directional ambiguity of the measured signal change are also disadvantageous issues. These have been well-understood by Lambeck et al. and they have proposed already in 1996 a fully integrated optical phase modulated Mach-Zehnder interferometer for biosensing (Lambeck et al., 1996). In this setup, a ZnO electro-optical modulator was integrated in each of the two interferometer arms (Figure 15). By applying oppositely controlled and well-calibrated driving voltages on the modulator electrodes, a continuous linear and periodic $\Delta\Phi_{\mathrm{mod}}$ phase difference sweep can be generated over an exact range of $0-2\pi$ between the modes propagating in the two arms. Supposing that the changes of the sample are not too fast compared to the modulation, eq. 4.5 can be rewritten for a period as:

$$I(t,\tau) = \frac{I_A}{2}\left\{1+\cos\left[2\pi\frac{L}{\lambda}(N_S(t)-N_R(t))+\Delta\Phi_0(\tau)+\Delta\Phi_0\right]\right\}+I_B, \quad (4.6)$$

where τ is the time variable within a modulation period and t is the experiment time. Setting aside $\Delta\Phi_0$ the actual phase of the interference response signal in the time-frame of a modulation period depends on the actual effective refractive index difference between the sensor and reference sensing areas measured at time point t. Consequently, an effective refractive index difference variation is related to the position shift of the quadrature points of the response signal. After filtering out the DC component, the phase information can be easily revealed by detecting only the time delay of the zero points in every modulation period. By individually optimizing all the components on the chip, the authors have demonstrated a phase-independent phase resolution of $1\times10^{-4}\times2\pi$ rad, which is equivalent to a detection limit of 5×10^{-8} for effective refractive index changes (Heideman and Lambeck, 1999). In the following 10 years, the setup was further developed and this value was improved to 5×10^{-9}, which corresponds to a resolution of 2×10^{-8} and 0.01 pg/mm^2 of bulk refractive index and surface mass density changes, respectively (Lambeck, 2006). More recently, other authors have reported different Mach-Zehnder interferometer biosensor configurations based on integrated electro-optical (Maisenhölder et al., 1997), magneto-optical (Sepúlveda et al., 2007) thermo-optical (Diemeer et al., 1999) or all-optical (Dér et al., 2010) phase modulations. As a great advantage of these phase modulated systems, the working principle allows detection without directional ambiguity, sensitivity fading and the need for an intensity calibration. However, the special manufacturing techniques and the application of non-standard materials, the electrodes and/or the (electrical) connections conflicting with microfluidics lead to a more increased complexity and in turn to cost increase and not to disposability. To overcome this drawback, an all-optical Mach-Zehnder interferometer has been recently introduced by Dante et al. (Dante et al., 2012). In this configuration, the phase is varied by modulation of emission wavelength of a commercial Fabry-Perot laser diode simply by changing its output power, periodically. The output signal of the sensor is analyzed with Fourier transform. The configuration neglecting any additional fabrication processes or electrical connections on the chip enables a measurement with all the advantages of the phase modulated interferometers mentioned above. The authors have reported a detection limit of 1.9×10^{-7} for bulk refractive index changes.

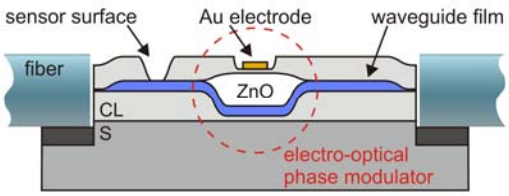

Figure 15: *Electro-optical phase modulated Mach-Zehnder interferometer of Heideman and Lambeck.* In this biosensor configuration, a ZnO electro-optical modulator is integrated in the interferometer arms in order to modulate the phase difference of the sensor and reference mode, continuously. This modulation allows detection without directional ambiguity, sensitivity fading and the need for an intensity calibration. The image is redrawn based on Ref. (Heideman and Lambeck, 1999).

As it was mentioned earlier, a typical drawback of fully integrated Mach-Zender interferometers compared to hybrid ones is the complexity of their waveguides, which results that the fabrication of their sensor chips is more technology- and in turn more cost-intensive. A recently developed hybrid Mach-Zehnder interferometer, the *grating coupled interferometer* continues the way pointed out by Heideman in 1991 (see the previous subchapter) by applying a simple planar waveguide. As it was published in 2009 by Kozma et al., this configuration is realized by the combination of an off-chip and an integrated optical unit (Kozma et al., 2009). The former comprises a laser source, two semi-transparent and two full mirrors in a modified Mach-Zehnder arrangement, in which a low cost but high quality liquid crystal phase modulator is inserted into one of the interferometer arms. By means of this unit, a phase modulated and a constant-phase beam separated from each other with a distance of a few millimeters are generated. These parallel beams are grating coupled into the integrated optical unit, i.e., the planar optical waveguide at two different coupling regions resulting in two propagating modes travelling towards the waveguide's edge, where a photodetector is placed (Figure 16). On the section between the two coupling regions, under the sensor surface, the phase modulated mode, i.e., the sensor mode propagates solely in the waveguide. On the one hand, a refractive index change of the sample of interest near the surface region shifts the phase of the sensor mode compared to that of the reference one. On the other hand, the liquid crystal modulator driven by a periodic square wave signal is being excited fast (in a few milliseconds) and it is relaxing slowly (in a few 10 milliseconds) in an exponential manner, while it is producing an additional and continuously changing phase shift of the sensor mode with an amplitude of $\Delta\Phi_{LCM} > 2\pi$. At the second coupling region, already within the waveguide, the combination of the two modes results in a time varying interference signal. Similarly to the interferometer of Lambeck et al., the information is in the

phase of this response signal, which can be revealed without directional ambiguity, sensitivity fading, or intensity calibration simply by fitting the following function to the slow sections of each period of the interference signal recorded by the photodetector:

$$I(t,\tau) = \frac{I_A}{2}\left\{1+\cos\left[2\pi\frac{L}{\lambda}N_S(t)+\Delta\Phi_{LCM}e^{-2\tau/\tau_c}-\Delta\Phi_{LCM}+\Delta\Phi_0\right]\right\}+I_B\ , \qquad (4.7)$$

where τ_c is a time constant characteristic to the LCM relaxation (Kozma et al., 2011a). The capabilities of the sensor were demonstrated in refractometric as well as biosensoric experiments and a detection limit of 9×10^{-7} and 0.5 pg/mm^2 were revealed for bulk refractive index and surface mass density changes, respectively (Kozma et al., 2011a). By the modification of the biosensor applying a new illumination method comprising a beam expander, a two-cell liquid crystal modulator and by using better optimized sensor chips with an extra outcoupling grating, Patko et al. have improved the resolution of grating coupled interferometer (Figure 16). In two-channel measurements, the refractive index changes of the ambient could be followed with a detection limit of 9×10^{-8} and the changes of surface mass density could be detected with a resolution of 0.05 pg/mm^2 (Patko et al., 2012). A commercial version of grating coupled interferometers presented here is launched onto the market by Creoptix in 2014.

Grating coupled interferometers have remarkable advantages over phase modulated Mach-Zehnder interferometers, since their planar waveguide chip is significantly simpler and easier to produce, which is important regarding e.g. disposability. Due to the working principle, neither directional ambiguity, nor sensitivity fading, nor need for calibration is a characteristic of grating coupled interferometers. Looking at their disadvantages, we have to highlight the drawback of hybrid Mach-Zehnder interferometers, namely, that the free-space sections, where the beams are propagating independently, have to be properly isolated from the effect of environmental noise or mechanical vibrations.

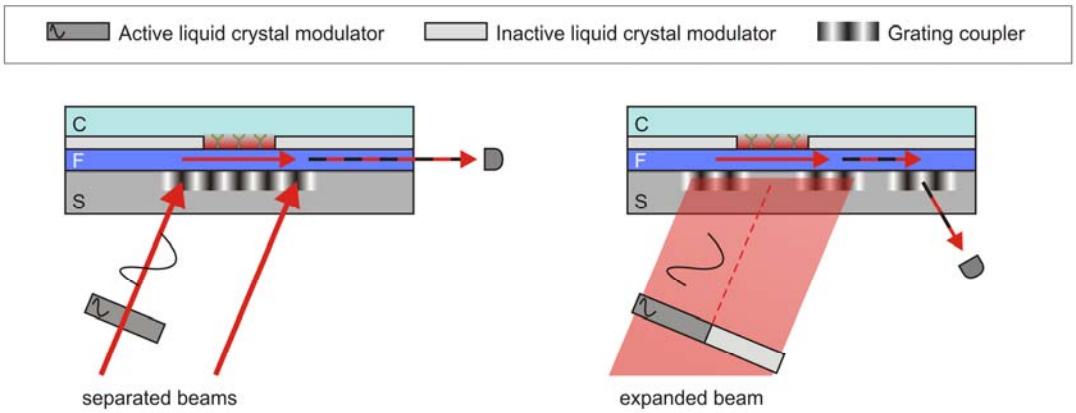

Figure 16: *Two versions of grating coupled interferometer.* A phase modulated and a not-modulated beam (left-hand side) or an expanded beam with phase modulated and not-modulated halves (right-hand side) are grating coupled into a planar waveguide. An effective refractive index change in the sensing region shifts the phase only of the (phase-modulated) sensor mode. After a few millimeters of propagation, in the second coupling region, the sensor mode is combined with the (not-modulated) reference mode resulting in their interference. The time varying interference signal is detected with a photodetector after coupling out the light from the waveguide.

Summarizing, it is important to note that, as a consequence of the working principle of all phase modulated waveguide interferometer introduced in this subchapter, their drawback compared to conventional Mach-Zehnder interferometers is, however, the significantly lower phase sampling rate, since a modulation period consisting of numerous data points has to be recorded in every case to evaluate the actual phase value. Thus, over the sampling rate, the modulation frequency is also a constraining factor, which can be a real issue in case of very fast changes at the sensor surface. Nevertheless, the recording of a period can be interpreted as data integration similar to that of data averaging in case of the sensors of the previous subchapter.

4.2.3. Young interferometers

We reviewed that in Mach-Zehnder interferometers, a beam modulation is necessary to avoid sensitivity fading, directional ambiguity and intensity calibration. It was also presented that this fact is not peculiar for Young interferometers, since their response signal is an interference pattern recorded by an image sensor and not a single intensity value detected with a photodetector. Consequently, simpler and in turn cheaper chips can be designed and higher phase acquisition rates can be achieved compared to e.g. those Mach-Zehnder interferometers, which are equipped with on-chip phase modulators. Similar to Mach-Zehnder interferometers, Young interferometers can also be realized based on slab as well as channel waveguides.

These different configurations have the advantage of ease of fabrication or improved possibilities in light guiding, respectively (see the previous chapters). A remarkable double path Young interferometer configuration, which follows the strategy of simplicity by aiming the application of relatively cheap and disposable slab waveguide sensor chips, is the dual polarization interferometry.

The first demonstration of dual polarization interferometry is related to Cross et al. in 1999. They presented the capabilities of a basic configuration in humidity sensing experiments (Cross et al., 1999). As a continuation of this work, four years later, the group has presented a significantly improved bench-top system designed for biosensoric applications and commercialized by Farfield Group (Cross et al., 2003). The sensor utilizes a multiple layer optical waveguide system, which is a vertically stacked five-layer dielectric consisting of two single-mode waveguide layers separated and covered with cladding material. The structure is deposited onto a bare silicon wafer. The input end-face of this dual slab waveguide is uniformly illuminated with the light of a coherent source, thus guided and radiation modes are induced in the waveguide and cladding materials, respectively. The radiation modes, which are not well confined in the single-mode waveguide layers, are scattering out from the sensor chip during the propagation. The lower waveguide is buried, the upper one is sampling the environment through openings of the upper cladding layer, therefore, the change of the sample results in a phase shift of the upper mode only. After propagating through the chip, the modes of the reference and sensing waveguide layers are coupled out by end-fire coupling (Figure 17). Since the end-facets of the waveguides are working as closely spaced apertures, an interference pattern is produced in the far-field, as it is common in Young interferometry, of which phase shift is related to the effective refractive index change of the upper waveguide. For this case, eq. 4.4 can be trivially rewritten as follows:

$$\Delta N_{TX_0}(t) = \left(\frac{\lambda}{L\Lambda}\right)\Delta u(t) = \left(\frac{\lambda}{2\pi L}\right)\Delta\Phi(t), \tag{4.8}$$

where TX_0 denotes TE_0 or TM_0 and Δu is the spatial shift of the interference fringes. A very important property of the presented setup is that it has a polarizer switch, which allows measuring both with TE_0 and TM_0 modes in a sequential manner. This feature helps to deeper understand the bio-chemical procedure of interest, since, based on the independent phase shift values gained from the interference signals of the two modes, the bulk refractive index changes can be separated from the surface mass density changes of the adlayer. For instance, also the conformation changes of the recognition elements in the sensing layer can be

monitored in this way, which enables a discrimination between affinity binding and non-specific adsorption (Swann et al., 2004). It is important to emphasize that two parallel openings are etched into the upper cladding layer, therefore, two-channel measurements can be performed in a biosensoric experiment. The detection limit of the commercialized instrument is about 10^{-7} and 0.1 pg/mm^2 for bulk refractive index and surface mass density changes, respectively (Estevez et al., 2012). Due to these advantageous properties, the capabilities of dual polarization interferometry have been widely exhausted during the last decade in different applications. Among others, the device has been efficiently used not only in biodetection experiments and protein interaction studies (Cross et al., 2003; Lin et al., 2006; Ricard-Blum et al., 2006; Swann et al., 2004), but it has also revealed interesting results in adsorbed or immobilized protein and DNA layer investigations (Berney and Oliver, 2005; Lu et al., 2004; Özalp, 2012; Sonesson et al., 2007; Zwang et al., 2010). Recently, a new design, a multiple path length dual polarization interferometry has been reported, which tries to solve the problem originated from the periodic nature of interference. Coffey et al. introduced a chip configuration, in which the two measurement channels have different lengths (Coffey et al., 2009). In practice, the channels are opened into each other and the length of the section between them decreases linearly from the length of the longer channel until that of the shorter one. The multiple path length and dual polarization measurement allows to determine the changes of thickness and refractive index values of even an ex situ modified chip surface. This is the case, if the TE and TM phase differences between the initial and final states are known for the channels, furthermore, if the opto-geometrical properties of the adlayer can be assumed to be uniform on the whole sensor surface. If a high degree of this homogeneity cannot be guaranteed, the number of 2π cycles cannot be reliably recalculated.

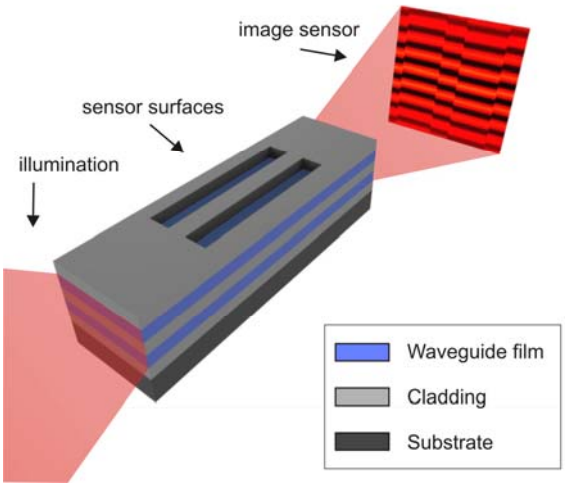

Figure 17: *Dual polarization interferometer*. The input end-face of this dual slab waveguide is uniformly illuminated in order to excite guided modes in the waveguide layers. The lower buried waveguide represents the reference arm of the interferometer, while the upper one samples the environment through openings of the upper cladding layer. After propagating through the chip, the modes are coupled out and an interference pattern is produced in the far-field.

Brandenburg and Henninger started in 1994 a different approach towards the development of an integrated biosensor (Brandenburg and Henninger, 1994). Their early efforts to apply channel waveguides for this purpose resulted that, in 2000, Brandenburg et al. presented their first Young interferometer designed for biosensing applications (Brandenburg et al., 2000). This setup comprises an integrated optical unit with a Y-junction and a cladding opening on the sensor as well as the reference arm. The light of a laser diode end-fire coupled into the integrated optical unit and split into two on the Y-junction propagates through the waveguide under the sensor and reference openings, respectively. The two beams are directed with a cylinder lens onto the surface of an image sensor, which records the resulting interference pattern. The evaluation of the interferograms using discrete Fourier transform permits to determine the phase shift, further the lateral shift of the interference fringes and the refractive index change occurred on the sensing region relative to that on the reference one. Testing its capabilities also in affinity binding measurements they revealed a detection limit of 9×10^{-8} and 0.75 pg/mm^2 (Brandenburg et al., 2000). The viability of the sensor configuration for measurement of analytes in blood plasma, monitoring of protein production as well as clinical diagnostics was also demonstrated (Brynda et al., 2002; Hoffmann et al., 2007; Nagel et al., 2008).

Wikerstal and Ymeti et al. have chosen basically the same strategy for biosensing, but they achieved lower limits of detection. Ymeti et al. have reported a phase and a bulk refractive index resolution of $1\times10^{-4}\times2\pi$ rad and 2×10^{-8}, respectively (Ymeti et al., 2002). Wikerstal has presented that this concept can be well-applied in three-channel measurements, as well (Wikerstal, 2001). Later, Ymeti et al. have published their results gained from a four-channel measurement (Ymeti et al., 2005, 2003). Later on, the sensing principle has been commercialized by Ostendum. Recently, as a continuation of the work presented in Ref. (Ymeti, 2004), a particularly interesting recent improvement of the same group is a multiple wavelength Young interferometer, with which a size selective detection has been proposed. Calculations predict similar sensing capabilities to that mentioned above (Mulder et al., 2012). The application of multiple wavelengths (similar to the application of multiple modes and polarizations) opens the possibility to derive refractive index changes from different regions, namely from different subsequent sublayers of the sample of interest above the sensing surface and at the same time to subtract the effect of bulk refractive index changes. The more independent the probes, the more detailed analysis of the adlayer can be performed. Similar results have been published by Kozma et al. applying spectroscopic ellipsometry (Kozma et al., 2011b).

Schmitt et al. have published a remarkable configuration for biosensing in 2005 (Schmitt et al., 2005). In their fully integrated Young interferometer, two parallel beams of a coherent light source are coupled into a waveguide through a broad grating coupler. The modes passed through the sensing and reference areas, respectively, are coupled out by a second grating and diffracted by a double slit. The Young fringes are recorded by means of an image sensor (Figure 18). The group has published a detection limit about an order of magnitude less than that of the aforementioned dual polarization interferometer, but recently, this value was further improved and in experimental investigation of surface bound bioreactions, a remarkable detection limit of 9×10^{-9} and 0.013 pg/mm^2 for bulk refractive index and surface mass density changes was revealed, respectively (Schmitt et al., 2007). To our best knowledge as well as based on other reviews (Estevez et al., 2012; Schmitt et al., 2008), this is the first configuration, with which a detection limit of 10^{-8} for bulk refractive index changes was surpassed.

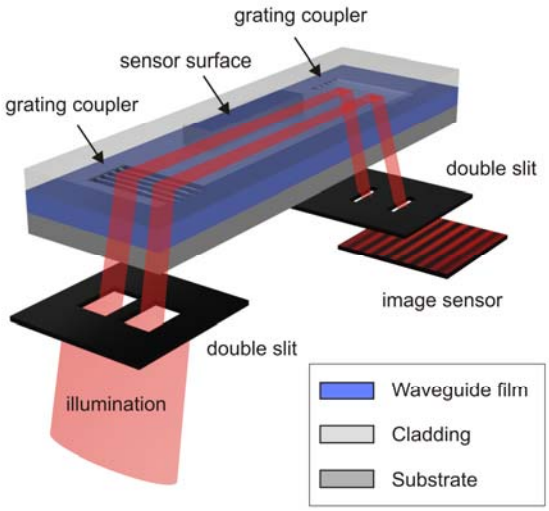

Figure 18: *Young interferometer of Schmitt et al.* Two parallel beams formed by a double slit are coupled into a waveguide through a broad grating coupler. One of the modes passes through the sensing area, while the other propagates through the reference path. After this, they are coupled out from the waveguide on a second grating. By means of a double slit, the modes are diffracted and an interference pattern is created, which is then recorded with an image sensor.

Alongside the indubitable advantages of Young interferometers detailed above, important drawbacks have to be mentioned as well. The distance between the end facet of the integrated optical part and the surface of the image sensor can be even a few centimeters in order to have an interference fringe period on the image sensor much larger than the pixel size and to cover all available pixels on the sensor surface with the interference pattern. However, the rays are propagating on this section in free-space, while, due to the environmental noise, the fluctuations of the ambient blur the fringes. The mechanical vibrations have a more significant effect on a system with long propagation paths. Consequently, a very effective isolation of the sensor from the environment is indispensable. As it is well-detailed in Ref. (Ymeti et al., 2003), the precise adjustment of the end facet – image sensor distance is necessary for multi-channel measurements with low detection limit. Moreover, cost-intensive image sensors, which even need energy-intensive cooling, have to be applied in order to achieve detection with high signal-to-noise ratio. These factors are disadvantageous in a completely integrated optical device designed for point-of-care applications.

5. Outlook and conclusions

The aim of the present review was to survey the developments of the past twenty years performed in the field of integrated planar optical waveguide interferometer biosensors. After a brief introduction in the underlying theory, various transducer configurations as well as miscellaneous read-out schemes have been presented, classified, compared and evaluated regarding their working principle, performance and applicability. As a summary, their most important parameters are collected in Table 1, additionally, the advantages peculiar to the major sub-groups of the biosensors in this paper, namely the common- and double path Mach-Zehnder and Young interferometers are highlighted in Figure 19.

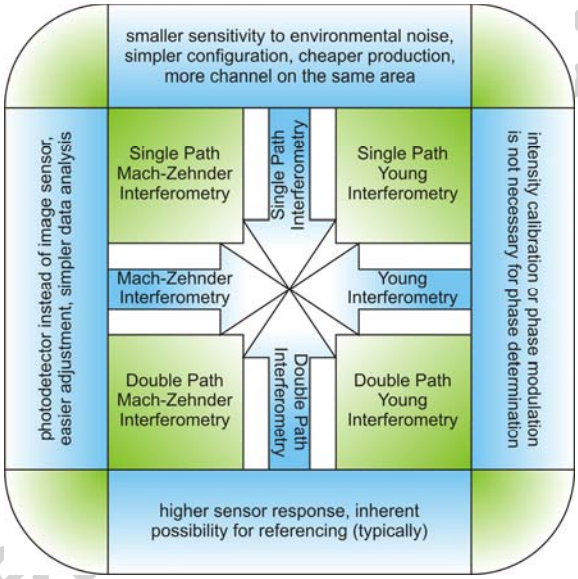

Figure 19: *Comparison of the four main groups of integrated planar optical waveguide interferometer biosensors*. The main advantages of different approaches, namely of common- and double path interferometry and Mach-Zehnder and Young interferometry are presented in the blue fields. The advantageous properties of a distinct field are valid for those main groups of planar optical waveguide interferometer biosensors, which are named in a neighboring green square.

As it was presented, the combination of the two very sensitive methods, namely interferometry and planar optical waveguide sensing led to a plurality of different label-free sensor with outstandingly low limits of detection and advantageous properties compared to other modern sensing schemes of the scientific literature. A plot in Figure 20 visualizes the time evolution of detection limit for bulk refractive index changes based on the values reported by the authors. As it is suggested by this graph and can be concluded from the

previous chapters, the capabilities of the different planar optical waveguide interferometer biosensors have been dynamically improved during the past twenty years. Without the need of directed transport of biomolecules onto individual nanoscale structures, the detection of even small molecules adsorbing or binding onto a macroscopic sensor surface is already possible. As it was reviewed, a detection limit of about 0.01 pg/mm^2 was already achieved. With the development of planar optical waveguide interferometers, this value will probably be further improved and even smaller or less concentrated analytes will be also detected. This sensitivity is attractive from the point of view of reagent consumption, as well. The lower detection limit can be achieved, the smaller amount of sample is needed for the measurement. Additionally, the relatively simple read-out principles and the compactness of these integrated optical transducers, which can be promoted as a single use consumable due to their relatively cheap high volume batch-manufacturability, make planar optical waveguide interferometers interesting not only for research, but for industrial applications, as well.

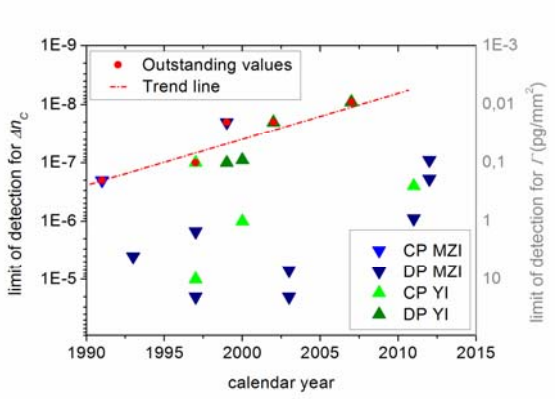

Figure 20: *Time evolution of detection limit of planar optical waveguide interferometer biosensors.* The detection limits for bulk refractive index changes of the biosensors presented in this review are plotted in the function of year of their publication. Common path (CP) and double path (DP) Young (YI) and Mach-Zehnder interferometers (MZI) are differentiated with triangles of different colors and orientations (see the legend in the lower right corner). A trend line is fitted to the outstanding values (marked with red spots). On the right axis of the graph, the detection limit for surface mass density changes is presented for approximate comparisons. Since the two sensitivities cannot be exactly compared (see the subchapter of "Sensing with evanescent field"), the ticks are deleted.

Nonetheless, until these integrated planar optical waveguide interferometer biosensors can be commercialized as point-of-care applications, serious improvements have to be performed in several aspects. On one hand, the technology still faces various challenges towards the integration in handheld devices, which could potentially be operated out of laboratory by

untrained personnel or even by the patient itself, such as in case of e.g. glucose sensors. The need for high quality, stable light sources, which are commonly still bulky and power demanding, furthermore, stabilized light coupling, efficient electrical and mechanical noise damping and highly effective temperature control in order to reduce the measurement noise make the recent configurations table top. Moreover, lacking waveguides with improved chemical and mechanical stability, the attenuation of parasitic effects, such as e.g. the drift of measurement signal, is challenging. On the other hand, correct liquid handling preferably in a lab-on-a-chip design, furthermore, stable surface chemistry with extended self-life, an accurate reproducibility and low non-specific binding need to be developed to eliminate a very complex and potentially wrong interpretation of the results. For high-throughput screening, the number of measurement channels has to be increased significantly, since in real multi-parameter analysis measurements, typically at least hundreds of parameters are investigated. For more detailed analysis of the adlayer changes on the sensor surface, multi-wavelength and multi-polarization measurements are indispensable. From a market perspective, the technology itself either has to find its very own niche or successfully compete with current labeled (e.g. fluorescent assays) as well as label-free (e.g. surface plasmon resonance) sensors and also by attaining more attention and acceptance in the community. Nevertheless, our criticism is not against this very promising technology. It is just to picture some incompleteness peculiar to the state-of-the-art. The authors believe that merging the on-going developments towards the aforementioned directions, planar optical waveguide interferometer biosensors have excellent prospects to appear in the close future even in point-of-care applications, as well.

Table 1: *Comprehensive table of integrated planar optical waveguide interferometer biosensors.* The table summarizes the most important parameters of the integrated planar optical waveguide interferometer biosensor configurations presented in this review. We note that the limit of detection values written in italic letters are estimations of the authors.

Authors	Biosensor	Configuration	Off-chip beam formation	Coupling	On-chip beam formation	Waveguide structure	Waveguide material	On-chip beam combination	Outcoupling	Off-chip beam combination	Phase modulation	Limit of detection	Reference
Lukosz and Stamm	Difference interferometer V1	Fully integrated common path MZI	Focusing	End-fire coupling	No	Step-index slab waveguide	TiO_2	No	End-fire coupling	Lens, beam splitter, Wollaston prisms	No	2×10^{-7} 0.13 pg/mm^2	(Lukosz and Stamm, 1991; Stamm and Lukosz, 1994)
Lukosz et al.	Difference interferometer V2	Fully integrated common path YI	Focusing	End-fire coupling	No	Step-index slab waveguide	TiO_2	No	End-fire coupling	Wollaston prism, polarizer	No	$\sim10^{-7}$ ~0.1 pg/mm^2	(Lukosz et al., 1997)
Lukosz et al.	Difference interferometer V3	Fully integrated common path YI	Focusing	End-fire coupling	No	Step-index slab waveguide	TiO_2	No	Grating	Lens, polarizer	No	$\sim10^{-7}$ ~0.1 pg/mm^2	(Lukosz et al., 1997)
Zinoviev et al.	Bimodal waveguide interferometer	Fully integrated common path MZI	Focusing	End-fire coupling	Modal splitter	Step-index ridge channel waveguide	Si_3N_4	No	End-fire coupling	No	No	2.5×10^{-7} 0.05 pg/mm^2	(Zinoviev et al., 2011)
Spinke et al.	Bidiffractive grating coupler	Fully integrated common path YI	TE and TM beam formation	Bidiffractive grating	No	Step-index slab waveguide	TiO_2	No	Bidiffractive grating	Lens, polarizer	No	*~10^{-5}* 24 pg/mm^2	(Spinke et al., 1997)
O'Brien et al.	Bidiffractive grating coupler	Fully integrated common path YI	TE and TM beam formation	Bidiffractive grating	No	Step-index slab waveguide	TiO_2	No	Bidiffractive grating	Lens, polarizer	No	*~10^{-6}* 6 pg/mm^2	(O'Brien et al., 2000)
Heideman et al.	Mach-Zehnder interferometer	Fully integrated double path MZI	Beam splitter	Grating	No	Step-index slab waveguide	Si_3N_4	No	Grating	Beam splitter	No	4×10^{-6} *~1 pg/mm^2*	(Heideman et al., 1993)
Ingenhoff et al.	Mach-Zehnder interferometer	Fully integrated double path MZI	Focusing	End-fire coupling	Y-junction	Graded-index diffused channel waveguide	Ag+ indiffused SiO_2	Y-junction	End-fire coupling	No	No	NA	(Ingenhoff et al., 1993)
Prieto et al.	Mach-Zehnder interferometer	Fully integrated Double path MZI	Focusing	End-fire coupling	Y-junction	Step-index rib channel waveguide	Si_3N_4	Y-junction	End-fire coupling	No	No	7×10^{-6} *~1 pg/mm^2*	(Prieto et al., 2003a)
Prieto et al.	ARROW Mach-Zehnder interferometer	Fully integrated double path MZI	Focusing	End-fire coupling	Y-junction	Step-index rib channel ARROW	Si_3N_4	Y-junction	End-fire coupling	No	No	2×10^{-5} *~10 pg/mm^2*	(Prieto et al., 2003b)
Brosinger et al.	Mach-Zehnder interferometer	Fully integrated double path MZI	Focusing	End-fire coupling	Two Y-junction	Step-index rib channel waveguide	SiON	Y-junction	End-fire coupling	No	No	2×10^{-5} *~10 pg/mm^2*	(Brosinger et al., 1997)
Drapp et al.	Mach-Zehnder interferometer	Fully integrated double path MZI	Focusing	End-fire coupling	Y-junction	Graded-index diffused channel waveguide	Ag+ exchanged SiO_2	3x3 coupler	End-fire coupling	No	No	1.5×10^{-6} *~1 pg/mm^2*	(Drapp et al., 1997)
Hartman et al.	Hartman interferometer	Fully integrated double path MZI	Broad beam formation	Grating	Channels	Step-index slab waveguide	Si_3N_4	Integrated optical elements	Grating	No	No	NA	(Hartman et al., 1995)
Heideman and Lambeck	Mach-Zehnder interferometer	Fully integrated double path MZI	Focusing	Fiber coupling	Y-junction	Step-index ridge channel waveguide	Si_3N_4	Y-junction	Fiber coupling	No	Integrated ZnO electro-optical modulator	2×10^{-8} 0.01 pg/mm^2	(Heideman and Lambeck, 1999)

Dante et al.	Mach-Zehnder interferometer	Fully integrated double path MZI	Focusing	End-fire coupling	Y-junction	Step-index rib channel waveguide	Si_3N_4	Y-junction	End-fire coupling	No	Wavelength modulation	1.9×10^{-7} *~0.1 pg/mm²*	(Dante et al., 2012)
Kozma et al.	Grating coupled interferometer V1	Hybrid double path MZI	Beam splitter	Grating	No	Step-index slab waveguide	Ta_2O_5	Grating	End-fire coupling	No	Liquid crystal modulator	9×10^{-7} 0.5 pg/mm²	(Kozma et al., 2011a)
Patko et al.	Grating coupled interferometer V2	Hybrid double path MZI	Beam expander	Grating	No	Step-index slab waveguide	Ta_2O_5	Grating	Grating	No	Liquid crystal modulator	9×10^{-8} 0.05 pg/mm²	(Patko et al., 2012)
Cross et al.	Dual polarization interferometer	Fully integrated double path YI	No	End-fire coupling	No	Step-index dual slab waveguide	Si_3N_4 doped SiO_2	No	End-fire coupling	No	No	1×10^{-7} 0.1 pg/mm²	(Estevez et al., 2012) (Cross et al., 2003)
Brandenburg et al.	Young interferometer	Fully integrated double path YI	Focusing	End-fire coupling	Y-junction	Step-index rib channel waveguide	SiON	No	End-fire coupling	Lens	No	9×10^{-8} 0.75 pg/mm²	(Brandenburg et al., 2000)
Ymeti et al.	Young interferometer	Fully integrated double path YI	Focusing	End-fire coupling	Y-junction	Step-index rib channel waveguide	Si_3N_4	No	End-fire coupling	Lens	No	2×10^{-8} *~0.01 pg/mm²*	(Ymeti et al., 2002)
Schmitt et al.	Integrated Young interferometer	Fully integrated double path YI	Beam splitter	Grating	No	Step-index slab waveguide	Ta_2O_5	No	Grating	Double slit	No	9×10^{-9} 0.013 pg/mm²	(Schmitt et al., 2007)

Acknowledgements

This work was funded by the Ministry of Economics and Europe of the State of Brandenburg and co-financed by the European Regional Development Fund (ERDF) of the European Union. Special thanks go to Dr. Róbert Horváth and Dániel Patkó, who encouraged us to write this review and who took the time and interest to support our work with their knowledge and by bringing some developments to our notice. The authors are very grateful to Dr. Kaspar Cottier and Harmen Mulder for reviewing the sections of grating coupled interferometer and young interferometers, respectively. The authors would also like to thank Andrea Zürcher and Milán Janosov for proofreading the manuscript and André Lehmann for rendering the 3D images.

References

Alivisatos, A.P., 2001. Less is More in Medicine. Sci. Am. September, 67–73.

Alocilja, E.C., Radke, S.M., 2003. Market analysis of biosensors for food safety. Biosens. Bioelectron. 18, 841–846.

Anderson, D.B., 1965. Application of semiconductor technology to coherent optical transducers and spatial filters, in: Tippett, J. (Ed.), Optical and Electro-Optical Information Processing. M.I.T. Press, Cambridge, pp. 221–234.

Bañuls, M.J., Puchades, R., Maquieira, A., 2013. Chemical surface modifications for the development of silicon-based label-free integrated optical (IO) biosensors: a review. Anal. Chim. Acta 777, 1–16.

Benaissa, K., Nathan, A., 1998. Silicon anti-resonant reflecting optical waveguides for sensor applications. Sensors Actuators A 65, 33–44.

Berney, H., Oliver, K., 2005. Dual polarization interferometry size and density characterisation of DNA immobilisation and hybridisation. Biosens. Bioelectron. 21, 618–626.

Brandenburg, A., 1996. Integrated optical interferometer for refreactometry and chemical sensing. Proc. SPIE 2783, 266–276.

Brandenburg, A., Henninger, R., 1994. Integrated optical Young interferometer. Appl. Opt. 33, 5941–5947.

Brandenburg, A., Krauter, R., Künzel, C., Stefan, M., Schulte, H., 2000. Interferometric sensor for detection of surface-bound bioreactions. Appl. Opt. 39, 6396–6405.

Brecht, A., Gauglitz, G., 1995. Optical probes and transducers. Biosens. Bioelectron. 10, 923–936.

Brosinger, F., Freimuth, H., Lacher, M., Ehrfeld, W., Gedig, E., Katerkamp, A., Spener, F., Cammann, K., 1997. A label-free affinity sensor with compensation of unspecific protein interaction by a highly sensitive integrated optical Mach–Zehnder interferometer on silicon. Sensors Actuators B Chem. 44, 350–355.

Brynda, E., Houska, M., Brandenburg, A., Wikersta, A., 2002. Optical biosensors for real-time measurement of analytes in blood plasma. Biosens. Bioelectron. 17, 665–675.

Busse, S., DePaoli, M., Wenz, G., Mittler, S., 2001. An integrated optical Mach–Zehnder interferometer functionalized by β-cyclodextrin to monitor binding reactions. Sensors Actuators B Chem. 80, 116–124.

Campbell, D.P., 2008. Interferometric Biosensors, in: Zourob, M., Souna, E., Turner, A.P.F. (Eds.), Principles of Bacterial Detection: Biosensors, Recognition Receptors and Microsystems. New York, pp. 169–211.

Chambers, J.P., Arulanandam, B.P., Matta, L.L., Weis, A., Valdes, J.J., 2008. Biosensor Recognition Elements. Curr. Issues Mol. Biol. 10, 1–12.

Chen, F., Wang, X., Wang, K., 2007. Development of ion-implanted optical waveguides in optical materials: A review. Opt. Mater. (Amst). 29, 1523–1542.

Ciminelli, C., Campanella, C.M., Dell'Olio, F., Campanella, C.E., Armenise, M.N., 2013. Label-free optical resonant sensors for biochemical applications. Prog. Quantum Electron. 37, 51–107.

Coffey, P.D., Swann, M.J., Waigh, T. a, Schedin, F., Lu, J.R., 2009. Multiple path length dual polarization interferometry. Opt. Express 17, 10959–10969.

Colladon, D., 1842. On the reflections of a ray of light inside a parabolic liquid stream. Comptes Rendus 15, 800–802.

Cooper, M.A., 2002. Optical Biosensors in Drug Discovery. Nat. Rev. Drug Discov. 1, 515–528.

Cottier, K., Wiki, M., Voirin, G., Gao, H., Kunz, R.E., 2003. Label-free highly sensitive detection of (small) molecules by wavelength interrogation of integrated optical chips. Sensors Actuators B Chem. 91, 241–251.

Cottier, M.K., 2004. Advanced Label-free Biochemical Sensors Based on Integrated Optical Waveguide Gratings. Universite de Neuchatel, Faculte des Sciences.

Cross, G.H., Reeves, A.A., Brand, S., Popplewell, J.F., Peel, L.L., Swann, M.J., Freeman, N.J., 2003. A new quantitative optical biosensor for protein characterisation. Biosens. Bioelectron. 19, 383–390.

Cross, G.H., Ren, Y., Freeman, N.J., 1999. Young's fringes from vertically integrated slab waveguides: Applications to humidity sensing. J. Appl. Phys. 86, 6483–6488.

Cunningham, B.T., 2009. Label-free optical biosensors: An introduction, in: Cooper, M.A. (Ed.), Label-Free Biosensors - Techniques and Applications. Camebridge University Press, New York, pp. 1–28.

Dakss, M.L., Kuhn, L., Heidrich, P.F., Scott, B.A., 1970. Grating coupler for efficient excitation of optical guided waves in thin films. Appl. Phys. Lett. 16, 523–525.

Dante, S., Duval, D., Sepúlveda, B., González-Guerrero, A.B., Sendra, J.R., Lechuga, L.M., 2012. All-optical phase modulation for integrated interferometric biosensors. Opt. Express 20, 7195–7205.

Davis, K.M., Miura, K., Sugimoto, N., Hirao, K., 1996. Writing waveguides in glass with a femtosecond laser. Opt. Lett. 21, 1729–1731.

De Feijter, J.A., Benjamins, J., Veer, F.A., 1978. Ellipsometry as a Tool to Study the Adsorption Behaviour of Synthetic and Biopolymers at the Air - Water Interface. Biopolimers 17, 1759–1772.

Debackere, P., Scheerlinck, S., Bienstman, P., Baets, R., 2006. Surface plasmon interferometer in silicon-on-insulator: novel concept for an integrated biosensor. Opt. Express 14, 7063–7072.

Dér, A., Valkai, S., Mathesz, A., Andó, I., Wolff, E.K., Ormos, P., 2010. Protein-based all-optical sensor device. Sensors Actuators B Chem. 151, 26–29.

Diemeer, M., De Dobbelaere, P., Flipse, R., 1999. Polymeric thermo-optical digital optical switches, in: Murphy, E.J. (Ed.), Integrated Optical Circuits and Components, Design and Applications. Taylor & Francis Inc, New York, pp. 239–303.

Drapp, B., Piehler, J., Brecht, A., Gauglitz, G., Luff, B.J., Wilkinson, J.S., Ingenhoff, J., 1997. Integrated optical Mach-Zehnder interferometers as simazine immunoprobes. Sensors Actuators B Chem. 38-39, 277–282.

Duguay, M.A., Kokubun, Y., Koch, T.L., Pfeiffer, L., 1986. Antiresonant reflecting optical waveguides in SiO2-Si multilayer structures. Appl. Phys. Lett. 49, 13–15.

Duval, D., Gonzalez-Guerrero, A.B., Dante, S., Dominguez, C., Lechuga, L.M., 2012a. Interferometric waveguide biosensors based on Si-technology for point-of-care diagnostic. Proc. SPIE 8431, 1–11.

Duval, D., González-Guerrero, A.B., Dante, S., Osmond, J., Monge, R., Fernández, L.J., Zinoviev, K.E., Domínguez, C., Lechuga, L.M., 2012b. Nanophotonic lab-on-a-chip platforms including novel bimodal interferometers, microfluidics and grating couplers. Lab Chip 12, 1987–1994.

Estevez, M.C., Alvarez, M., Lechuga, L.M., 2012. Integrated optical devices for lab-on-a-chip biosensing applications. Laser Photon. Rev. 6, 463–487.

Fan, X., White, I.M., Shopova, S.I., Zhu, H., Suter, J.D., Sun, Y., 2008. Sensitive optical biosensors for unlabeled targets: a review. Anal. Chim. Acta 620, 8–26.

Fattinger, C., 1993. The bidiffractive grating coupler. Appl. Phys. Lett. 62, 1460–1462.

Fattinger, C., Mangold, C., Gale, M.T., Schütz, H., 1995. Bidiffractive grating coupler: universal transducer for optical interface analytics. Opt. Eng. 34, 2744–2753.

Guillod, T., Kehl, F., Hafner, C., 2013. FEM-based method for the simulation of dielectric waveguide grating biosensors. Prog. Electromagn. Res. 137, 565–583.

Gut, K., 2012. A suggestion of utilizing bimodal layers of the polymer SU8 for the purpose of monitoring the changes in the refractive index. Opt. Appl. 42, 407–416.

Hamori, A., Nagy, N., 2004. Sub-micrometer period refractive index grating coupler for single mode optical waveguide sensors. Sensors Proc. IEEE 3, 1333–1336.

Hartman, N.F., Campbell, D., Gross, M., 1988. Waveguide interferometer configurations. Proc. IEEE-LEOS '88 (Laser Electro-Optics Soc. Ann. Meet.), St. Clara, CA, USA 298–299.

Hartman, N.F., Wyvill, J.C., Campbell, D., Edmonds, P., 1995. Rapid response biosensor for detection and identification of common foodborne pathogens. Proc. SPIE 2345, 128–137.

Hecht, J., 1999. Guiding light and lumious fountains, in: City of Light: The Story of Fiber Optics. Oxford University Press, New York, pp. 12–27.

Heideman, R.G., Kooyman, R.P.H., Greve, J., 1991. Development of an optical waveguide interferometric immunosensor. Sensors Actuators B Chem. 4, 297–299.

Heideman, R.G., Kooyman, R.P.H., Greve, J., 1993. Performance of a highly sensitive optical waveguide Mach-Zehnder interferometer immunosensor. Sensors Actuators B 10, 209–217.

Heideman, R.G., Lambeck, P. V., 1999. Remote opto-chemical sensing with extreme sensitivity: design, fabrication and performance of a pigtailed integrated optical phase-modulated Mach-Zehnder interferometer system. Sensors Actuators B 61, 100–127.

Hoffmann, C., Schmitt, K., Brandenburg, A., Hartmann, S., 2007. Rapid protein expression analysis with an interferometric biosensor for monitoring protein production. Anal. Bioanal. Chem. 387, 1921–1932.

Holford, T.R.J., Davis, F., Higson, S.P.J., 2012. Recent trends in antibody based sensors. Biosens. Bioelectron. 34, 12–24.

Homola, J., Yee, S.S., Guaglitz, G., 1999. Surface plasmon resonance sensors: review. Sensors Actuators B 54, 3–15.

Horvath, R., Pedersen, H.C., Skivesen, N., Selmeczi, D., Larsen, N.B., 2005. Monitoring of living cell attachment and spreading using reverse symmetry waveguide sensing. Appl. Phys. Lett. 86, 071101.

Hua, P., Luff, B.J., Quigley, G.R., Wilkinson, J.S., Kawaguchi, K., 2002. Integrated optical dual Mach–Zehnder interferometer sensor. Sensors Actuators B Chem. 87, 250–257.

Huber, W., Barner, R., Fattinger, C., Hübscher, J., Koller, H., Müller, F., Schlatter, D., Lukosz, W., 1992. Direct optical immunosensing (sensitivity and selectivity). Sensors Actuators B 6, 122–126.

Hunt, H.K., Armani, A.M., 2014. Bioconjugation strategies for label-free optical microcavity sensors. IEEE J. Sel. Top. Quantum Electron. 20, 6900213.

Ingenhoff, J., Drapp, B., Gauglitz, G., 1993. Biosensors using integrated optical devices. Fresenius. J. Anal. Chem. 346, 580–583.

Jackson, J.D., 1998a. Plane Electromagnetic Waves and Wave Propagation, in: Classical Electrodinamics. John Wiley & Sons, Inc., New York, pp. 295–351.

Jackson, J.D., 1998b. Waveguides, resonant cavities and optical fibers, in: Classical Electrodinamics. John Wiley & Sons, Inc., New York, pp. 352–406.

Jain, K.K., 2005. Nanotechnology in clinical laboratory diagnostics. Clin. Chim. Acta 358, 37–54.

Jenkins, F.A., White, H.E., 1957a. The Superposition of Waves, in: Fundamentals of Optics. McGraw-Hill Book Company, New York, pp. 211–231.

Jenkins, F.A., White, H.E., 1957b. The Double Slit, in: Fundamentals of Optics. McGraw-Hill Book Company, New York, pp. 311–327.

Jiménez, D., Bartolomé, E., Moreno, M., Muñoz, J., Domínguez, C., 1996. An integrated silicon ARROW Mach-Zehnder interferometer for sensing applications. Opt. Commun. 132, 437–441.

Joannopoulos, J.D., Johnson, S.G., Winn, J.N., Meade, R.D., 2008. Photonic Crystals: Molding the Flow of Light, 2nd ed, Wild. Princeton University Press, Princeton and Oxford.

Justino, C.I.L., Rocha-Santos, T.A., Duarte, A.C., 2010. Review of analytical figures of merit of sensors and biosensors in clinical applications. Trends Anal. Chem. 29, 1172–1183.

Klenkar, G., Liedberg, B., 2008. A microarray chip for label-free detection of narcotics. Anal. Bioanal. Chem. 391, 1679–1688.

Kovacs, N., Patko, D., Orgovan, N., Kurunczi, S., Ramsden, J.J., Vonderviszt, F., Horvath, R., 2013. Optical anisotropy of flagellin layers: in situ and label-free measurement of adsorbed protein orientation using OWLS. Anal. Chem. 85, 5382–5389.

Kozma, P., Hamori, A., Cottier, K., Kurunczi, S., Horvath, R., 2009. Grating Coupled Interferometry for Optical Sensing. Appl. Phys. B 97, 5–8.

Kozma, P., Hamori, A., Kurunczi, S., Cottier, K., Horvath, R., 2011a. Grating coupled optical waveguide interferometer for label-free biosensing. Sensors Actuators B 155, 446–450.

Kozma, P., Kozma, D., Németh, A., Jankovics, H., Kurunczi, S., Horvath, R., Vonderviszt, F., Fried, M., Petrik, P., 2011b. In-depth characterization and computational 3D reconstruction of flagellar filament protein layer structure based on in situ spectroscopic ellipsometry measurements. Appl. Surf. Sci. 257, 7160–7166.

Kozma, P., Lehmann, a., Wunderlich, K., Michel, D., Schumacher, S., Ehrentreich-Förster, E., Bier, F.F., 2013. A novel handheld fluorescent microarray reader for point-of-care diagnostic. Biosens. Bioelectron. 47, 415–420.

Kunz, R.E., Cottier, K., 2006. Optimizing integrated optical chips for label-free (bio-)chemical sensing. Anal. Bioanal. Chem. 384, 180–190.

Lambeck, P.V., 2006. Integrated optical sensors for the chemical domain. Meas. Sci. Technol. 17, R93–R116.

Lambeck, P.V., Heideman, R.G., Ikkink, T.J., 1996. Phase-modulated Mach-Zehnder Interferometer for sensor applications. Med. Biol. Eng. Comput. 34, 145–146.

Lazcka, O., Del Campo, F.J., Muñoz, F.X., 2007. Pathogen detection: a perspective of traditional methods and biosensors. Biosens. Bioelectron. 22, 1205–17.

Levy, R., Ruschin, S., 2009. Design of a single-channel modal interferometer waveguide sensor. IEEE Sens. J. 9, 146–153.

Lin, S., Lee, C.K., Lin, Y.H., Lee, S.Y., Sheu, B.C., Tsai, J.C., Hsu, S.M., 2006. Homopolyvalent antibody-antigen interaction kinetic studies with use of a dual-polarization interferometric biosensor. Biosens. Bioelectron. 22, 715–721.

Long, G.L., Winefordner, J.D., 1983. Limit of Detection A Closer Look at the IUPAC Definition. Analalytical Chem. 55, 712–724.

Lu, J.R., Swann, M.J., Peel, L.L., Freeman, N.J., 2004. Lysozyme Adsorption Studies at the Silica/Water Interface Using Dual Polarization Interferometry. Langmuir 20, 1827–1832.

Luff, B.J., Wilkinson, J.S., Piehler, J., Hollenbach, U., Ingenhoff, J., Fabricius, N., 1998. Integrated Optical Mach – Zehnder Biosensor. J. Light. Technol. 16, 583–592.

Lukosz, W., 1991. Principles and sensitivities of integrated optical and surface plasmon sensors for direct affinity sensing and immunosensing. Biosens. Bioelectron. 6, 215–225.

Lukosz, W., 1995. Integrated optical chemical and direct biochemical sensors. Sensors Actuators B Chem. 29, 37–50.

Lukosz, W., Stamm, C., 1991. Integrated optical interferometeras relative humidity sensor and differential refractometer. Sensors Actuators A 25, 185–188.

Lukosz, W., Stamm, C., Moser, H.R., Ryf, R., Dübendorfer, J., 1997. Difference interferometer with new phase-measurement method as integrated-optical refractometer, humidity sensor and biosensor. Sensors Actuators B 38-39, 316–323.

Mach, L.Z., 1892. Über einen Interferenzrefraktor. Instrumentenkunde 12, 89–94.

Maisenhölder, B., Zappe, H.P., Kunz, R.E., Riel, P., Moser, M., Edlinger, J., 1997. A GaAs/AlGaAs-based refractometer platform for integrated optical sensing applications. Sensors Actuators B 38-39, 324–329.

Marcatili, E.A.J., 1969. Dielectric Rectangular Waveguide and Directional Coupler for Integrated Optics. Bell Syst. Tech. J. 48, 2071–2102.

Mulder, H.K.P., Ymeti, A., Subramaniam, V., Kanger, J.S., 2012. Size-selective detection in integrated optical interferometric biosensors. Opt. Express 20, 20934–20950.

Nagel, T., Ehrentreich-Förster, E., Singh, M., Schmitt, K., Brandenburg, A., Berka, A., Bier, F.F., 2008. Direct detection of tuberculosis infection in blood serum using three optical label-free approaches. Sensors Actuators B Chem. 129, 934–940.

Nakadate, S., 1988. Phase detection of equidistant fringes for highly sensitive optical sensing: Principle and error analyses. J. Opt. Soc. Am. A 5, 1258–1264.

Nakadate, S., 1990. High precision retardation measurement using phase detection of Young's fringes. Appl. Opt. 29, 242–246.

O'Brien, T., Johnson, L.H., Aldrich, J.L., Allen, S.G., Liang, L., Plummer, A.L., Krak, S.J., Boiarski, A.A., 2000. The development of immunoassays to four biological threat agents in a bidiffractive grating biosensor. Biosens. Bioelectron. 14, 815–828.

O'Malley, S., 2008. Recent Advances in Label-free Biosensors Applications in Protein Biosynthesis and HTS screening. Protein Biosynthesis, Nova Science Publishers Inc.

Oliver, N.S., Toumazou, C., Cass, A.E.G., Johnston, D.G., 2009. Glucose sensors: a review of current and emerging technology. Diabet. Med. 26, 197–210.

Osterberg, H., Smith, L.W., 1964. Transmission of Optical Energy Along Surfaces: Part II, Inhomogeneous Media. J. Opt. Soc. Am. 54, 1078–1079.

Özalp, V.C., 2012. Dual-polarization interferometry for quantification of small molecules using aptamers. Anal. Bioanal. Chem. 402, 799–804.

Parriaux, O., Veldhuis, G.J., 1998. Normalized analysis for the sensitivity optimization of integrated optical evanescent-wave sensors. J. Light. Technol. 16, 573–582.

Patko, D., Cottier, K., Hamori, A., Horvath, R., 2012. Single beam grating coupled interferometry: high resolution miniaturized label-free sensor for plate based parallel screening. Opt. Express 20, 23162–23173.

Peng, S.T., Tamir, T., Bertoni, H.L., 1975. Theory of Periodic Dielect Waveguides. IEEE Trans. Microw. Theory Tech. 23, 123–133.

Prieto, F., Llobera, A., Jiménez, D., Dominguez, C., Calle, A., Lechuga, L.M., 2000. Design and analysis of silicon antiresonant reflecting optical waveguides for evanscent field sensor. J. Light. Technol. 18, 966–972.

Prieto, F., Sepúlveda, B., Calle, A., Llobera, A., Domínguez, C., Abad, A., Montoya, A., Lechuga, L.M., 2003a. An integrated optical interferometric nanodevice based on silicon technology for biosensor applications. Nanotechnology 14, 907–912.

Prieto, F., Sepúlveda, B., Calle, A., Llobera, A., Domínguez, C., Lechuga, L.M., 2003b. Integrated Mach–Zehnder interferometer based on ARROW structures for biosensor applications. Sensors Actuators B Chem. 92, 151–158.

Ricard-Blum, S., Peel, L.L., Ruggiero, F., Freeman, N.J., 2006. Dual polarization interferometry characterization of carbohydrate-protein interactions. Anal. Biochem. 352, 252–259.

Saleh, B.E.A., Teich, M.C., 2007. Guided-wave optics, in: Fundamentals of Photonics. John Wiley & Sons, Inc., Hoboken, New Jersey, pp. 289–324.

Schipper, E.F., Brugman, A.M., Dominguez, C., Lechuga, L.M., Kooyman, R.P.H., Greve, J., 1997. The realization of an integrated Mach-Zehnder waveguide immunosensor in silicon technology. Sensors Actuators B Chem. 40, 147–153.

Schlatter, D., Barner, R., Fattinger, C., Huber, W., Hübscher, J., Hurst, J., Koller, H., Mangold, C., Müller, F., 1993. The difference interferometer: application as a direct affinity sensor. Biosens. Bioelectron. 8, 109–116.

Schmitt, K., Oehse, K., Sulz, G., Hoffmann, C., 2008. Evanescent field Sensors Based on Tantalum Pentoxide Waveguides – A Review. Sensors 8, 711–738.

Schmitt, K., Schirmer, B., Brandenburg, A., 2005. Label-free detection of biomolecules by waveguide interferometry. Proc. SPIE 5855, 459–462.

Schmitt, K., Schirmer, B., Hoffmann, C., Brandenburg, A., Meyrueis, P., 2007. Interferometric biosensor based on planar optical waveguide sensor chips for label-free detection of surface bound bioreactions. Biosens. Bioelectron. 22, 2591–2597.

Schneider, B.H., Dickinson, E.L., Vach, M.D., Hoijer, J.V., Howard, L.V., 2000a. Highly sensitive optical chip immunoassays in human serum. Biosens. Bioelectron. 15, 13–22.

Schneider, B.H., Dickinson, E.L., Vach, M.D., Hoijer, J.V., Howard, L.V., 2000b. Optical chip immunoassay for hCG in human whole blood. Biosens. Bioelectron. 15, 597–604.

Schneider, B.H., Edwards, J.G., Hartman, N.F., 1997. Hartman interferometer: versatile integrated optic sensor for label-free, real-time quantification of nucleic acids, proteins, and pathogens. Clin. Chem. 43, 1757–1763.

Sepúlveda, B., Armelles, G., Lechuga, L.M., 2007. Magneto-optical phase modulation in integrated Mach–Zehnder interferometric sensors. Sensors Actuators A Phys. 134, 339–347.

Sheehan, P.E., Whitman, L.J., 2005. Detection limits for nanoscale biosensors. Nano Lett. 5, 803–807.

Snyder, A.W., Love, J.D., 1983. Optical Waveguide Theory, October. Chapman and Hall Ltd, London.

Sonesson, A.W., Callisen, T.H., Brismar, H., Elofsson, U.M., 2007. A comparison between dual polarization interferometry (DPI) and surface plasmon resonance (SPR) for protein adsorption studies. Colloids surfaces B 54, 236–40.

Spinke, J., Oranth, N., Fattinger, C., Koller, H., Mangold, C., Voegelin, D., 1997. The bidiffractive grating coupler: application to imnxunosensing. Sensors Actuators B 38-39, 256–260.

Squires, T.M., Messinger, R.J., Manalis, S.R., 2008. Making it stick: convection, reaction and diffusion in surface-based biosensors. Nat. Biotechnol. 26, 417–426.

Stamm, C., Dangel, R., Lukosz, W., 1998. Biosensing with the integrated-optical difference interferometer: dual-wavelength operation. Opt. Commun. 153, 347–359.

Stamm, C., Lukosz, W., 1993. Integrated optical difference interferometer as refractometer and chemical sensor. Sensors Actuators B Chem. 11, 177–181.

Stamm, C., Lukosz, W., 1994. Integrated optical difference interferometer as biochemical sensor. Sensors Actuators B 18-19, 183–187.

Swann, M.J., Peel, L.L., Carrington, S., Freeman, N.J., 2004. Dual-polarization interferometry: an analytical technique to measure changes in protein structure in real time, to determine the stoichiometry of binding events, and to differentiate between specific and nonspecific interactions. Anal. Biochem. 329, 190–198.

Tamir, T., 1975. Beam and waveguide couplers, in: Integrated Optics. Springer Berlin Heildelberg, pp. 83–137.

Tamir, T., Peng, S.T., 1977. Analysis and design of grating couplers. Appl. Phys. 14, 235–254.

Tiefenthaler, K., Lukosz, W., 1984. Integrated optical switches and gas sensors. Opt. Lett. 9, 137–139.

Tiefenthaler, K., Lukosz, W., 1988. Sensitivity of grating couplers as integrated-optical chemical sensors. J. Opt. Soc. Am. B 6, 209–220.

Tien, P.K., 1977. Integrated optics and new wave phenomena. Rev. Mod. Phys. 49, 361–420.

Tsunoda, K., Kikuchi, S., Nomura, K., Aizawa, K., Okamoto, K., Akaiwa, H., 1999. Characteristics of sensor response of a difference interferometric slab optical waveguide refractive index sensor with a prism coupling method. Anal. Sci. 15, 241–247.

Turner, A.P.F., 2000. Biosensors - sense and sensitivity. Science (80-.). 290, 1315–1317.

Updike, S.J., Hicks, G.P., 1967. The Enzyme Electrode. Nature 214, 986–988.

Vörös, J., Ramsden, J.J., Csúcs, G., Szendrő, I., De Paul, S.M., Textor, M., Spencer, N.D., 2002. Optical grating coupler biosensors. Biomaterials 23, 3699–3710.

Weisser, M., Tovar, G., Mittler-Neher, S., Knoll, W., Brosinger, F., Freimuth, H., Lacher, M., Ehrfeld, W., 1999. Specific bio-recognition reactions observed with an integrated Mach-Zehnder interferometer. Biosens. Bioelectron. 14, 405–411.

Wikerstal, A., 2001. Multichannel solutions for optical labelfree detection schemes based on the interferometric and grating coupler principle, Ph.D. dissertation. University of Freiburg, Freiburg, Germany.

Ymeti, A., 2004. Development of a multichannel integrated Young interferometer immunosensor. Ph.D. Thesis, University of Twente.

Ymeti, A., Kanger, J.S., Greve, J., Besselink, G.A.J., Lambeck, P.V., Wijn, R., Heideman, R.G., 2005. Integration of microfluidics with a four-channel integrated optical Young interferometer immunosensor. Biosens. Bioelectron. 20, 1417–1421.

Ymeti, A., Kanger, J.S., Greve, J., Lambeck, P.V., Wijn, R., Heideman, R.G., 2003. Realization of a multichannel integrated Young interferometer chemical sensor. Appl. Opt. 42, 5649–5660.

Ymeti, A., Kanger, J.S., Wijn, R., Lambeck, P.V., Greve, J., 2002. Development of a multichannel integrated interferometer immunosensor. Sensors Actuators B Chem. 83, 1–7.

Young, T., 1804. Experiments and Calculations Relative to Physical Optics. Philos. Trans. R. Soc. London 94, 1–16.

Zehnder, L.Z., 1891. Ein neuer Interferenzrefraktor. Instrumentenkunde 11, 275–285.

Zinoviev, K., Carrascosa, L.G., Sánchez del Río, J., Sepúlveda, B., Domínguez, C., Lechuga, L.M., 2008. Silicon Photonic Biosensors for Lab-on-a-Chip Applications. Adv. Opt. Technol. 2008, 1–6.

Zinoviev, K.E., González-Guerrero, A.B., Domínguez, C., Lechuga, L.M., 2011. Integrated bimodal waveguide interferometric biosensor for label-free analysis. J. Light. Technol. 29, 1926–1930.

Zwang, T.J., Fletcher, W.R., Lane, T.J., Johal, M.S., 2010. Quantification of the Layer of Hydration of a Supported Lipid Bilayer. Langmuir 26, 4598–4601.

Authors	Biosensor	Configuration	Off-chip beam formation	Coupling	On-chip beam formation	Waveguide structure	Waveguide material	On-chip beam combination	Outcoupling	Off-chip beam combination	Phase modulation	Limit of detection	Reference
Lukosz and Stamm	Difference interferometer V1	Fully integrated common path MZI	Focusing	End-fire coupling	No	Step-index slab waveguide	TiO_2	No	End-fire coupling	Lens, beam splitter, Wollaston prisms	No	2×10^{-7} 0.13 pg/mm^2	(Lukosz and Stamm, 1991; Stamm and Lukosz, 1994)
Lukosz et al.	Difference interferometer V2	Fully integrated common path YI	Focusing	End-fire coupling	No	Step-index slab waveguide	TiO_2	No	End-fire coupling	Wollaston prism, polarizer	No	$\sim10^{-7}$ ~0.1 pg/mm^2	(Lukosz et al., 1997)
Lukosz et al.	Difference interferometer V3	Fully integrated common path YI	Focusing	End-fire coupling	No	Step-index slab waveguide	TiO_2	No	Grating	Lens, polarizer	No	$\sim10^{-7}$ ~0.1 pg/mm^2	(Lukosz et al., 1997)
Zinoviev et al.	Bimodal waveguide interferometer	Fully integrated common path MZI	Focusing	End-fire coupling	Modal splitter	Step-index ridge channel waveguide	Si_3N_4	No	End-fire coupling	No	No	2.5×10^{-7} 0.05 pg/mm^2	(Zinoviev et al., 2011)
Spinke et al.	Bidiffractive grating coupler	Fully integrated common path YI	TE and TM beam formation	Bidiffractive grating	No	Step-index slab waveguide	TiO_2	No	Bidiffractive grating	Lens, polarizer	No	*~10*$^{-5}$ 24 pg/mm^2	(Spinke et al., 1997)
O'Brien et al.	Bidiffractive grating coupler	Fully integrated common path YI	TE and TM beam formation	Bidiffractive grating	No	Step-index slab waveguide	TiO_2	No	Bidiffractive grating	Lens, polarizer	No	*~10*$^{-6}$ 6 pg/mm^2	(O'Brien et al., 2000)
Heideman et al.	Mach-Zehnder interferometer	Fully integrated double path MZI	Beam splitter	Grating	No	Step-index slab waveguide	Si_3N_4	No	Grating	Beam splitter	No	4×10^{-6} *~1 pg/mm*^{2}	(Heideman et al., 1993)
Ingenhoff et al.	Mach-Zehnder interferometer	Fully integrated double path MZI	Focusing	End-fire coupling	Y-junction	Graded-index diffused channel waveguide	Ag+ indiffused SiO_2	Y-junction	End-fire coupling	No	No	NA	(Ingenhoff et al., 1993)
Prieto et al.	Mach-Zehnder interferometer	Fully integrated Double path MZI	Focusing	End-fire coupling	Y-junction	Step-index rib channel waveguide	Si_3N_4	Y-junction	End-fire coupling	No	No	7×10^{-6} *~1 pg/mm*^{2}	(Prieto et al., 2003a)
Prieto et al.	ARROW Mach-Zehnder interferometer	Fully integrated double path MZI	Focusing	End-fire coupling	Y-junction	Step-index rib channel ARROW	Si_3N_4	Y-junction	End-fire coupling	No	No	2×10^{-5} *~10 pg/mm*^{2}	(Prieto et al., 2003b)
Brosinger et al.	Mach-Zehnder interferometer	Fully integrated double path MZI	Focusing	End-fire coupling	Two Y-junction	Step-index rib channel waveguide	SiON	Y-junction	End-fire coupling	No	No	2×10^{-5} *~10 pg/mm*^{2}	(Brosinger et al., 1997)
Drapp et al.	Mach-Zehnder interferometer	Fully integrated double path MZI	Focusing	End-fire coupling	Y-junction	Graded-index diffused channel waveguide	Ag+ exchanged SiO_2	3x3 coupler	End-fire coupling	No	No	1.5×10^{-6} *~1 pg/mm*^{2}	(Drapp et al., 1997)
Hartman et al.	Hartman interferometer	Fully integrated double path MZI	Broad beam formation	Grating	Channels	Step-index slab waveguide	Si_3N_4	Integrated optical elements	Grating	No	No	NA	(Hartman et al., 1995)
Heideman and Lambeck	Mach-Zehnder interferometer	Fully integrated double path MZI	Focusing	Fiber coupling	Y-junction	Step-index ridge channel waveguide	Si_3N_4	Y-junction	Fiber coupling	No	Integrated ZnO electro-optical modulator	2×10^{-8} 0.01 pg/mm^2	(Heideman and Lambeck, 1999)
Dante et al.	Mach-Zehnder interferometer	Fully integrated double path MZI	Focusing	End-fire coupling	Y-junction	Step-index rib channel waveguide	Si_3N_4	Y-junction	End-fire coupling	No	Wavelength modulation	1.9×10^{-7} *~0.1 pg/mm*^{2}	(Dante et al., 2012)
Kozma et al.	Grating coupled interferometer V1	Hybrid double path MZI	Beam splitter	Grating	No	Step-index slab waveguide	Ta_2O_5	Grating	End-fire coupling	No	Liquid crystal modulator	9×10^{-7} 0.5 pg/mm^2	(Kozma et al., 2011a)
Patko et al.	Grating coupled interferom	Hybrid double path MZI	Beam expander	Grating	No	Step-index slab	Ta_2O_5	Grating	Grating	No	Liquid crystal modulat	9×10^{-8} 0.05 pg/m	(Patko et al., 2012)

	eter V2					waveguide					or	m^2	
Cross et al.	Dual polarization interferometer	Fully integrated double path YI	No	End-fire coupling	No	Step-index dual slab waveguide	Si_3N_4 doped SiO_2	No	End-fire coupling	No	No	1×10^{-7} 0.1 pg/mm^2	(Estevez et al., 2012) (Cross et al., 2003)
Brandenburg et al.	Young interferometer	Fully integrated double path YI	Focusing	End-fire coupling	Y-junction	Step-index rib channel waveguide	SiON	No	End-fire coupling	Lens	No	9×10^{-8} 0.75 pg/mm^2	(Brandenburg et al., 2000)
Ymeti et al.	Young interferometer	Fully integrated double path YI	Focusing	End-fire coupling	Y-junction	Step-index rib channel waveguide	Si_3N_4	No	End-fire coupling	Lens	No	2×10^{-8} *~0.01 pg/mm*^{2}	(Ymeti et al., 2002)
Schmitt et al.	Integrated Young interferometer	Fully integrated double path YI	Beam splitter	Grating	No	Step-index slab waveguide	Ta_2O_5	No	Grating	Double slit	No	9×10^{-9} 0.013 pg/mm^2	(Schmitt et al., 2007)

Highlights

1) The recent potentials and limitations of biosensors are outlined.

2) Integrated planar optical waveguide interferometer biosensors are reviewed in depth.

3) Their theoretical background is summarized in a comprehensive way.

4) The various configurations are reviewed in a systematic and categorical manner.

5) A summary outlines and compares the properties of the presented approaches.